TRENDS IN SCIENCES 2026; 23(5): 12000
https://doi.org/10.48048/tis.2026.12000 RESEARCH ARTICLE

Encapsulation of *Nelumbo nucifera* Leaf Extract in Chitosan for Improved Antioxidant and Anti-breast Cancer Activities Against MCF-7 Cell Lines Through PI3K/mTOR Inhibition

Khairani Fitri[1,*], Marwan Saad Azzubaidi[2] and Nurulhuda Mat Hassan[2]

[1]*Department of Pharmacy, Faculty of Pharmacy and Health, Institut Kesehatan Helvetia, Medan 20124, Indonesia*
[2]*Department of Pharmacology, Faculty of Medicine, Universiti Sultan Zainal Abidin, Kampus Kota, Kuala Terengganu 20400, Malaysia*

([*]Corresponding author's e-mail: khairanifitri0201@gmail.com)

Received: 23 September 2025, Revised: 7 October 2025, Accepted: 17 October 2025, Published: 1 January 2026

Abstract

The development of plant extracts as a phytomedicine is an emerging trend in the pharmaceutical industry. This study aimed to synthesize *Nelumbo nucifera* leaf extract (NL) into chitosan nanoparticles by ionic gelation using sodium trypolyphosphate as the cross-linking agent. The characteristic of *Nelumbo nucifera* leaf extract loaded into chitosan encapsulate (NLCE) was analyzed for encapsulation efficiency (UV-Vis), particle size and polydispersity (PSA), morphology (SEM), chemical interaction (FTIR), phytochemical profile (LC-HRMS), and thermal stability (DSC). In addition, the biological activity of NLCE was conducted using antioxidant and anti-breast cancer activity against MCF-7 cells. Subsequently, the NLCE formed spherical particles with a size range of 200 - 600 nm (median of 350 nm, PI of 1.07). The FTIR analysis illustrated the reaction between chitosan and TPP at 1,315 cm^{-1} as a stretching vibration of the P = O group, while LC-HRMS confirmed the presence of secondary metabolites, including erteberel, hyperoside, 5,7-dihydroxy-2-(2,3,4-trihydroxyphenyl)-4H-chromen-4-one, miquelianin, 2-(3,4-dihydroxyphenyl)-5,7-dihydroxy-4-oxo-4H-chromen-3-yl 6-O-β-D-xylopyranosyl-β-D-glucopyranoside, and senkyunolide B. NLCE also exhibited good stability under high temperature. Additionally, the NLCE demonstrated an antioxidant activity against DPPH and ABTS radicals dependent on concentration manner. The inhibitory concentration 50 (IC_{50}) of NLCE showed better antioxidant properties than NL and chitosan. Similar to the antioxidant properties, the NLCE demonstrated cytotoxic and antiproliferation effects dependent on concentration manner against MCF-7 cells. The anti-breast cancer effect of NLCE was revealed by cell cycle arrest induction in G2/M phases, which promotes apoptosis of MCF-7 cells. As a mechanism, the NLCE promoted inhibition of PI3K and mTOR proteins, that known as regulators of cell cycle and apoptosis in cancer cells. Overall, these findings confirm the successful development of NLCE with enhanced physicochemical stability and potent biological activities. NLCE represents a promising phytomedicine value of chitosan-based nanoencapsulation to improve the bioactivity and therapeutic prospects of plant-derived compounds.

Keywords: *Nelumbo nucifera*, Nanoencapsulation, Antioxidant, Breast cancer, Cell cycle arrest, Apoptosis, PI3K/mTOR

Introduction

Nelumbo nucifera, commonly referred to simply as lotus, is an aquatic plant from the family Nelumbonaceae, widely cultivated in Asia and Africa [1]. At present, the green leaves of the plant are increasingly favoured in Asia for its application as a tea and dietary supplement for weight loss, cholesterol reduction, cardiovascular regulation, and antioxidant properties [2-4]. Additionally, the leaves of lotus have been predominantly exploited in traditional Chinese medicine to address burns, diarrhoea, perspiration, haemorrhage, and fever [5]. Contemporary pharmacological research has shown that *N. nucifera*

leaves possess a diverse array of biological actions, including antihyperlipidemic, antidiabetic, antiobesity, antioxidant, anticancer, and liver-protective properties, among others [6,7]. The major medically advantageous properties of *N. nucifera* are attributed to its components. Diverse compounds in several chemical categories have been extracted from this plant, including alkaloids, flavonoids, glycosides, and triterpenoids [8]. Flavonoids constitute the primary medicinal components of *N. nucifera* leaves, with numerous compounds discovered, including quercetin, kaempferol, leucocyanidin, leucodelphinidin, catechin, isoquercitrin, and astragalin [9]. Nonetheless, a significant drawback is their volatility throughout the preparation, transport, storage, and consumption of food. Many variables, including temperature, light, pH, enzymes, and other nutrients, can destroy them, so reducing their function and possible health advantages [10]. The technique of encapsulation is employed to prevent these events, enabling the entrapment of active chemicals within a substance, hence enhancing their absorption into the body and allowing the therapeutic use of plant extracts [11].

The plant-based component, a phenolic molecule, is safeguarded by particles and can be utilised in the production of nutraceutical functional meals within the pharmaceutical and cosmetic industries. Regarding the polymers that are applied for encapsulation, chitosan, formed of β-(1-4)-linked D-glucosamine (deacetylated unit) and N-acetyl-D-glucosamine (acetylated unit), exhibits optimal properties, being biodegradable, biocompatible, nontoxic, and cost-effective [12-14]. The production and processing of chitosan particles can occur through various methods, with ionic gelation being one of the most prevalent [15]. The encapsulation of plant extracts and essential oils in chitosan nanoparticles has been described [16,17]. Nonetheless, there is a lack of knowledge regarding the incorporation of *N. nucifera* leaf extract into chitosan nanoparticles. Encapsulation of a particular molecule from the extract is advantageous; nevertheless, separation techniques increase costs and may result in low extraction yields in certain instances [18]. Moreover, it has been reported that the amalgamation of several components in an extract can produce a beneficial interaction, resulting in an enhancement of biological function due to their collaborative action [19]. According to Morales-Olán *et al.* [20], the chitosan-encapsulated chia extract showed an enhancement in DPPH radical inhibition. Furthermore, Ukwubile *et al.* [21] indicated that the anticancer efficacy of *Curcuma longa* extract with encapsulated chitosan against MCF-7 cells was enhanced relative to the unencapsulated form. This demonstrates the efficacy of chitosan encapsulation in enhancing the antioxidant and anticancer properties of the extract.

This research was motivated by the pressing necessity to discover novel methods for enhancing the extract's efficacy in breast cancer treatment. The researchers aim to enhance treatment and support for individuals impacted by this difficulty through the exploration of creative solutions. Encapsulating *N. nucifera* extract in chitosan represents a promising strategy that may yield synergistic effects by integrating the antioxidant and anticancer properties of curcumin and chitosan. This approach embodies current progress in nanomedicine, which seeks to utilise the distinctive properties of nanoparticles. This facilitates more accurate and efficient therapy by inhibiting the deterioration of the extract's active constituents while minimising adverse effects.

Materials and methods

Plant materials and extraction

The research materials for this study include *Nelumbo nucifera* leaf obtained from Marelan, North Sumatera, Indonesia. The N. nucifera leaf was authenticated by Herbarium Medanese, Universitas Sumatera Utara (Voucher ID: 250/UN5.1.1.2/PPM.1/2023). The desiccated sample was extracted employing a solid-liquid extraction method, according to parameters of 55 h (extraction duration), 70% (hydroalcohol concentration), and a 1:11 w/v (solid to solvent ratio). The extraction of *N. nucifera* leaves involved dissolving the dry powder of the leaf samples in a solvent for a specified duration and solid-to-solvent ratio. Subsequent to the extraction phase, the filtrate was gathered and subjected to evaporation via a rotary evaporator to yield a crude extract (NL). Consequently, the extract was stored in a glass bottle at 4 °C before to use [22].

Synthesis of *N. nucifera* leaf extract-loaded chitosan encapsulate

The *N. nucifera* leaf extract-loaded chitosan encapsulates (NLCE) were fabricated via the ionic gelation technique, renowned for its simplicity and efficacy in encapsulating bioactive substances. Low molecular weight chitosan was initially dissolved in a 1% w/v acetic acid solution while maintaining continual agitation to produce a homogeneous chitosan solution. The solution was agitated for several hours to guarantee total disintegration. Sodium tripolyphosphate (TPP) was independently synthesized as the cross-linking agent by dissolving it in distilled water at a concentration of 1% w/v. The NL (2% w/v) was combined with the chitosan solution in a ratio of 1:1, respectively. Afterwards, the TPP solution was added dropwise under vigorous stirring, promoting ionic contact between the positively charged amino groups of chitosan and the negatively charged phosphate groups of TPP. This interaction resulted in the spontaneous generation of NLCE. The stirring operation was continued for 60 min to guarantee homogeneous particle size and complete reaction. The resultant NLCEs were obtained through centrifugation and subsequently washed multiple times with distilled water to eliminate unreacted substances. The encapsulates were either freeze-dried or low-temperature oven-dried to achieve a powdered form, which was subsequently stored in a desiccator for future use [23].

Characterization of *N. nucifera* leaf extract-loaded chitosan encapsulate

The encapsulation efficiency of the process was determined by comparing the total phenolic content of NLCE with that of NL. Briefly, a specified amount of NLCE was dissolved in 1% (v/v) acetic acid with agitation to release the encapsulated extract. The solution underwent centrifugation, and the supernatant was obtained for examination. The total phenolic content (TPC) in the supernatant was measured using the Folin-Ciocalteu method, employing gallic acid as the standard reference. Absorbance was quantified at 765 nm utilizing a UV-Vis spectrophotometer. Encapsulation efficiency was determined using Eq. (1) [24].

$$\text{Encapsulation efficiency (\%)} = \frac{\text{TPC encapsulated}}{\text{TPC extract}} \times 100 \quad (1)$$

where TPC encapsulated denotes the phenolic content within the dissolved NLCE, and TPC initial represents the overall phenolic substance employed for encapsulation. All measurements were conducted in duplicate to ensure precision.

Meanwhile, the particle dimensions and distribution of NLCE were assessed utilizing a particle size analyzer. Prior to examination, a tiny amount of the desiccated microcapsules was dispersed in distilled water or a suitable dispersion medium. The dispersion was sonicated for several minutes to inhibit aggregation and achieve a homogeneous suspension. The prepared sample was subsequently placed into the sample holder of the particle size analyzer. The device was calibrated to the specified operational settings, and the findings were documented and examined to evaluate the uniformity and appropriateness of the NLCE. Both differential and cumulative volume distribution (Q3) were recorded to determine the median particle diameter (d_{50}) and polydispersity index (PDI) [25].

Subsequently, the surface morphology of NLCE was analyzed using scanning electron microscopy (SEM). Before examination, the dried NLCE were affixed to an aluminum SEM stub with a conductive glue. The mounted specimen was thereafter coated with a thin layer of gold or platinum via a sputter coater to augment conductivity and mitigate charging under the electron beam. The coated sample was placed inside the SEM chamber and operated at an accelerating voltage of 10 kV and 5,000× magnification. High-resolution photos were obtained to examine the surface texture, morphology, and structural integrity of the NLCE [26].

In addition, the chemical reaction in this process was assessed under Fourier Transform Infrared (FTIR) and Liquid Chromatography High Resolution Mass Spectrum (LC-HRMS). The NLCE was analyzed using an FTIR spectrometer (Bruker Vertex 70, Germany). The data were documented within the wavenumber range of 4,000 to 500 cm^{-1} [27]. Meanwhile, LC-HRMS was performed to determine the phytochemical compounds containing in NLCE. The analysis was carried out on a Thermo Scientific Q Exactive Orbitrap MS equipped with an electrospray ionization (ESI)

source operated in negative ion mode. Chromatographic separation was achieved on a C18 reversed-phase column (2.1×100 mm^2, 1.7 µm) at 40 °C. The mobile phases consisted of (A) 0.1% formic acid in water and (B) acetonitrile, with a gradient elution was 0 - 1 min, 5%, B; 1 - 10 min, linear increase to 40% B; 10 - 18 min, linear increases to 95% B; held at 95% for 2 min; returned to 5% B over 1 min and equilibrated for 3 min. The flow rate was set at 0.3 mL/min, and the injection volume was 5 µL. The MS conditions included a scan range of m/z 100 - 1,000, resolution at 70,000, sheath gas flow rate of 35 arb, auxiliary gas flow rate of 10 arb, spray voltage of –3.0 kV, and capillary temperature of 320 °C. For MS/MS fragmentation, a normalized collision energy of 30 eV was applied in data-dependent acquisition mode. Compound identification was based on comparison of accurate mass-to-charge ratios (m/z) in the $[M-H]^-$ ion form, retention times, and, where available, fragmentation patterns, with entries in the METLIN and HMDB spectral databases [28].

Furthermore, the thermal properties of NLCE were analyzed using DSC. First, approximately 10 mg of the sample was weighed and placed in an aluminum DSC pan. Samples were heated from room temperature to a designated upper temperature limit (400 °C) at a constant rate (10 °C/min) under a nitrogen atmosphere. DSC thermograms were recorded to observe any endothermic or exothermic transitions, indicating changes in the thermal stability and structural properties of the microcapsules. These transitions provided insights into the EE and thermal behavior of the active compounds within the chitosan matrix [29].

DPPH and ABTS radical scavenging activities

The DPPH radical-scavenging assay was used to assess the antioxidant activity of the NLCE, NL, and chitosan encapsulate without extract (CE). First, a 0.1 mM DPPH solution was prepared in methanol and was shielded from light to avoid deterioration. Different concentrations (31.25 - 500 µg/mL) of each sample solution were prepared by dissolving the samples in methanol. Each sample concentration was combined with an equivalent volume of DPPH solution in a test tube, yielding a final DPPH concentration appropriate for assessing antioxidant activity. The mixtures were incubated in the dark at room temperature for 30 min to facilitate the reaction between the DPPH radicals and antioxidants in the sample. After incubation, the absorbance of each sample was measured at 517 nm using a spectrophotometer. The reduction in absorbance signified the scavenging of DPPH free radicals, and the percentage of radical inhibition was calculated using Eq. (2) [30].

$$\text{Percentage inhibition (\%)} = \frac{\text{Absorbance of control} - \text{absorbance of sample}}{\text{Absorbance of control}} \times 100 \quad (2)$$

Meanwhile, the antioxidant activity of the NLCE, NL, and CE was further evaluated using the ABTS radical-scavenging assay. The ABTS radical cation ($ABTS^{\bullet+}$) solution was initially produced by combining 7 mM ABTS with 2.45 mM potassium persulfate. The mixture was allowed to react in the dark at ambient temperature for 12 - 16 h to produce stable ABTS radicals, yielding a blue-green solution. Prior to the experiment, the ABTS solution was diluted with ethanol or PBS to achieve an absorbance of approximately 0.7 at 734 nm. Different concentrations (31.25 - 500 µg/mL) of the microcapsules were prepared in methanol, and each concentration was combined with $ABTS^{\bullet+}$ solution at a 1:1 ratio in a test tube. Each combination was incubated in the dark at room temperature for 6 min to allow the antioxidants in the extract to neutralize the ABTS radicals. After incubation, the absorbance of each sample was measured at 734 nm with a spectrophotometer. The percentage inhibition of ABTS radicals was calculated using Equation 4. These 2 assessments were using ascorbic acid (AA) as a positive control [31].

Cell culture

Breast cancer cells (MCF-7 cells) were obtained from the Parasitology Laboratory, Universitas Gadjah Mada, Yogyakarta. MCF-7 cells were cultured in Dulbecco's Modified Eagle Medium (DMEM) with 10% (v/v) fetal bovine serum, 100 U/mL penicillin, and 100 µg/mL streptomycin at 37 °C with 5% CO_2.

Cytotoxic effect of *N. nucifera* leaf extract-loaded chitosan encapsulates

This study was conducted in 4 groups test group including NLCE, NL, CE, and doxorubicin (positive control). The standard procedure was applied to determine the cytotoxic effect of the samples. Briefly,

the MCF-7 cells were inoculated into 96-well plates at a density of 1×10^4 cells per well and incubated overnight at 37 °C in a humidified environment with 5% CO_2 to facilitate cell adhesion. Following a 24-hour period, the cells were subjected to treatment with different quantities of samples between 31.25 to 500 µg/mL, formulated in culture media. Untreated cells functioned as a negative control, whilst doxorubicin was administered as a conventional cytotoxic drug in a similar concentration to the sample. After 24 h of incubation, the media was substituted with 100 µL of new media containing 0.5 mg/mL MTT reagent and incubated for an additional 3 - 4 h at 37 °C. Subsequently, the resultant formazan crystals were solubilized by the addition of 100 µL of dimethyl sulfoxide (DMSO) to each well, and the absorbance was quantified at 570 nm utilizing a microplate reader. Cell viability was quantified as a percentage compared to the control group [32].

Cell cycle arrest induces activity

Cell cycle distribution of MCF-7 cells following treatment with NLCE, NL, CE, and doxorubicin was analyzed using flow cytometry with propidium iodide (PI) staining. MCF-7 cells were seeded in 6-well plates at a density of 2×10^5 cells/well and allowed to attach for 24 h. The cells were then treated with each sample at IC_{50} for another 24 h. After treatment, cells were harvested by trypsinization, washed twice with cold phosphate-buffered saline (PBS), and fixed in 70% ice-cold ethanol at −20 °C overnight. The fixed cells were washed again with PBS, resuspended in 500 µL of staining solution containing 50 µg/mL propidium iodide and 100 µg/mL RNase A, and incubated at 37 °C for 30 min in the dark. Samples were analyzed using a flow cytometer (BD FACSCalibur™, BD Biosciences, USA), and at least 10,000 events per sample were recorded [33].

Apoptosis induces activity

The induction of apoptosis in MCF-7 cells by all sample tests was assessed using dual staining with Annexin V-FITC and propidium iodide (PI), followed by flow cytometric analysis. MCF-7 cells were seeded in 6-well plates at 2×10^5 cells/well and treated with IC_{50} of each sample for 24 h. Untreated cells were used as negative controls. After treatment, both floating and adherent cells were collected, washed twice with cold PBS, and resuspended in 100 µL of 1× Annexin V binding buffer. Then, 5 µL of Annexin V-FITC and 5 µL of propidium iodide (50 µg/mL) were added to each sample. The mixture was incubated in the dark for 15 min at room temperature. Following incubation, 400 µL of binding buffer was added to each sample, and the cells were analyzed immediately using a flow cytometer (BD FACSCalibur™, BD Biosciences). A total of 10,000 cells were acquired per sample. The percentage of viable, early apoptotic, late apoptotic, and necrotic cells was quantified using quadrant analysis with FlowJo™ software [34].

PI3K/mTOR expression using a flow cytometer

MCF-7 cells were inoculated into 6-well plates at a density of 2×10^5 cells per well and permitted to adhere overnight. The cells were subsequently exposed to each sample at an IC_{50} for 24 h under usual culture conditions. Untreated cells served as negative controls. Subsequent to treatment, cells were collected via trypsinization, rinsed twice with cold phosphate-buffered saline (PBS), and fixed with 4% paraformaldehyde for 15 min at ambient temperature. The cells were subsequently rinsed and permeabilized with 0.1% Triton X-100 in PBS for 10 min to facilitate intracellular antibody access. Subsequently, permeabilized cells were treated with fluorochrome-conjugated primary antibodies targeting PI3K and mTOR (e.g., anti-PI3K-Alexa Fluor® 488 and anti-mTOR-PE, BD Biosciences) for 30 min at ambient temperature in the absence of light. Following staining, cells were rinsed with PBS and resuspended in 300 µL of PBS for acquisition. Data were acquired via a BD FACSCalibur™ flow cytometer, with a minimum of 10,000 events per sample. Fluorescence intensities were assessed with FlowJo™ software to ascertain relative protein expression levels in comparison to untreated control cells. Results were presented as mean fluorescence intensity (MFI), and statistical analyses were conducted to assess the significance of protein downregulation [35].

Statistical analysis

All experiments were performed in triplicate (n = 3), and the results are presented as mean ± standard

deviation (SD). Graphs also include error bars to represent SD. Statistical differences were analyzed using 1-way ANOVA followed by Tukey's post hoc test in GraphPad Prism version 8.0.1 (GraphPad software, USA), and values of $p < 0.05$ were considered significantly different.

Results and discussion

Characteristics of *N. nucifera* leaf extract-loaded chitosan encapsulates

In this study, the sodium tripolyphosphate was employed as a crosslinker between chitosan and NL. The NLCE was obtained at approximately 2.50 g with unique organoleptic properties as presented in **Table 1**. The organoleptic of NLCE is described in powder form with a brown-green color. This color is not significantly different from NL and confirms that NL contributed to the synthesis process. Additionally, the odor is still native to the NL, specific to the extract characteristic. Additional characterization was conducted by assessing encapsulation efficiency (%EE). The investigation indicated that NL contained 26.35 ± 2.04 mg GAE/g extract, whereas NLCE contained 23.18 ± 2.55 mg GAE/g NLCE. The calculation of encapsulation efficiency resulted in a percentage of 87.56 ± 1.30%. The %EE quantifies the efficacy of encapsulating the active ingredient, specifically the extract, within the microcapsule matrix, represented as the total phenolic content of the NLCE. Prior research has indicated that various parameters can affect %EE, including quantities of chitosan, extract, and TPP; reaction duration; solution pH; reaction temperature; and stirring velocity [36]. Generally, augmenting chitosan concentration tends to enhance encapsulation efficiency up to a specific threshold. An increased concentration of chitosan in the solution enhances the matrix's ability to retain the extract within the microcapsules [37]. Chitosan functions as a polymer that constitutes the capsule wall; thus, increased concentrations facilitate the development of denser and thicker capsule layers. Nevertheless, excessive concentration markedly elevates the viscosity of the chitosan solution, impeding dispersion and resulting in irregular capsule formation or agglomeration, thereby diminishing %EE [38]. Moreover, augmenting the extract concentration typically enhances the quantity of active substances encapsulated within the microcapsules, albeit only to a limited degree. At ideal extract concentrations, %EE can be elevated due to the direct correlation between the quantity of extract retained in the microcapsule and its capacity [39]. Nevertheless, if the extract concentration is excessively high, the surplus may "overload" the capsules, resulting in unencapsulated active ingredients that could precipitate or be lost during manufacture [40]. This diminishes the total energy efficiency. Additionally, TPP acts as a crosslinking agent, interacting with chitosan to create a capsule wall. A precise TPP concentration is necessary for adequate cross-linking to create a stable and effective capsule. At low TPP concentrations, the cross-links established between TPP and chitosan lack sufficient strength to render the capsule wall more flimsy and facilitate the release of active substances, hence diminishing %EE. Nevertheless, excessive TPP content may hinder optimal chitosan binding, leading to an overly thick capsule shape that diminishes its capacity to retain the extract [41-43].

Table 1 Organoleptic and encapsulation efficiency of *N. nucifera* leaf extract-loaded chitosan encapsulates.

Test	Result	
	NL	**NLCE**
Color	Brown less	Brown-green
Odor	Specific extract	Specific extract
Shape	Thick	Powder
TPC (mg GAE/g sample	26.35 ± 2.04	23.18 ± 2.55
EE (%)	NI	87.56 ± 1.30

NL (*Nelumbo nucifera* leaf extract); NLCE (*N. nucifera* leaf extract-loaded chitosan encapsulates); TPC (total phenolic content); TFC (total flavonoid content); EE (encapsulation efficiency); NI (not identified).

The study results depicted in **Figure 1** indicate that NLCE has a size range of 0.20 to 0.60 µm, characterized by a rather narrow distribution curve. The median value (d50) was measured at 0.35 µm, with d10 and d90 recorded at 0.20 µm and 0.55 to 0.60 µm, respectively, signifying that most particles fell within the nanometer to submicrometer range. The polydispersity index (PI) data indicate that NLCE is rather uniformly distributed, with a PI of 1.07. This study demonstrates that the methods of encapsulation and homogenization are successful in generating uniformly sized particles and reducing the occurrence of big agglomerates. Particle sizes under 500 nm are anticipated to boost system stability, augment surface area, and improve the bioavailability of the active component encapsulated inside the chitosan matrix, hence facilitating its prospective use as an effective bioactive delivery system [20].

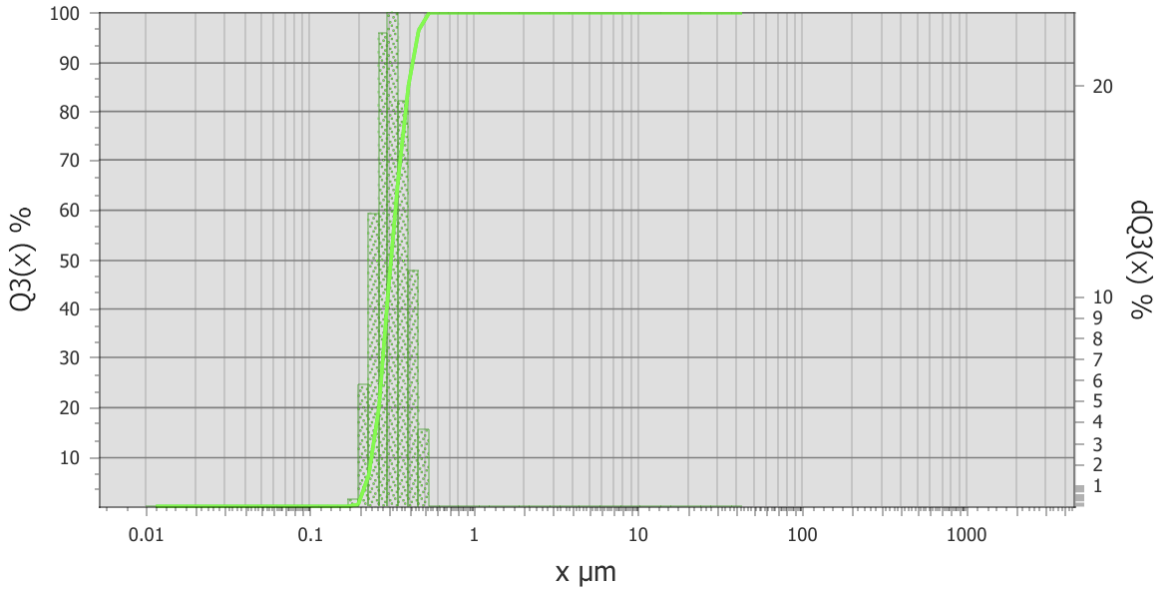

Figure 1 Particle size distribution of NLCE determined by a Particle Size Analyzer (PSA). The cumulative volume curve (Q3, solid line) and differential distribution (bars) show particle sizes ranging from 0.20 to 0.60 µm, with a median diameter (d50) of approximately 0.35 µm. Data are expressed as mean ± SD from triplicate measurements (n = 3).

The morphology of NLCE was examined using SEM to corroborate these results, as illustrated in **Figure 2**. SEM analysis at 5,000× magnification demonstrated distinct variations among the enclosed materials (**Figures 2(A) - 2(D)**). **Figure 2(A)** illustrates the morphology of the extract, characterized by a smooth surface with several elongated fissures, signifying an amorphous nature devoid of a characteristic crystalline structure. **Figure 2(B)** illustrates the shape of chitosan, which is porous and exhibits uneven aggregation, indicative of a polymer matrix generated post-drying. **Figure 2(C)** illustrates the morphology of Na-TPP as crisp flakes or crystals, aligning with the crystalline characteristics of inorganic salts. Simultaneously, the shape of NLCE (**Figure 2(D)**) reveals globular aggregates with a textured surface, devoid of distinct TPP crystals, signifying the successful ionic interaction between chitosan and TPP that constitutes the matrix encapsulating the extract. The results align with the particle size distribution analysis conducted by a Particle Size Analyzer (PSA), revealing a size range of 0.20 - 0.60 µm, a median (d50) of 0.35 µm, and a polydispersity index of roughly 1.07. This size falls between the nanoparticle-submicron range with a rather narrow dispersion, signifying a stable and uniform capsule structure. The homogeneous globular morphology evident in the SEM results corroborates the PSA data, indicating that the majority of particles are under 500 nm in size, hence anticipated to enhance the stability, surface area, and bioavailability of the active component encapsulated inside the chitosan matrix.

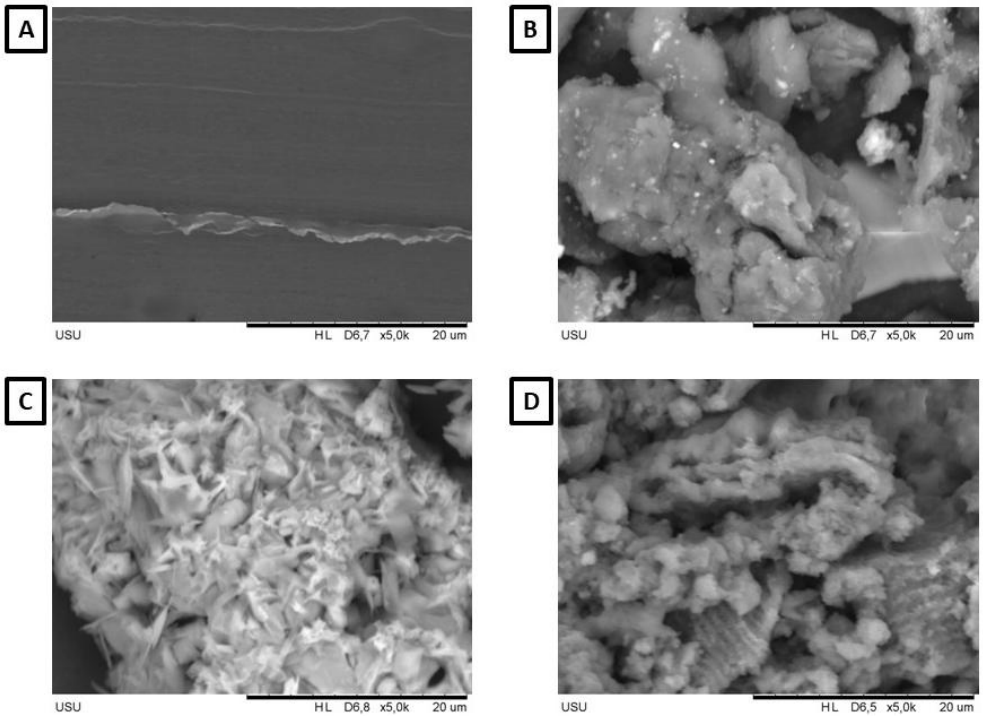

Figure 2 Scanning electron micrographs (5,000×, scale bar = 20 µm) of the sample. (A) *N. nucifera* leaf extract, (B) chitosan exhibiting a porous gel-like morphology, (C) sodium trypolyphosphate displaying irregular crystalline fragments, and (D) NLCE presenting aggregated globular particles, indicating successful ionic crosslinking between chitosan and TPP, entrapping the extract. Images are representative of 3 independent preparations (n = 3).

The findings on the particle distribution and morphology analysis of NLCE align with previously reported data. A prior work indicated that CS-TPP microcapsules encapsulating carvacrol exhibited a diameter ranging from 532 to 716 nm [44]. The size of CS-TPP microcapsules containing *Satureja hortensis* essential oil was 192 nm [45]. Furthermore, CS-TPP microcapsules, including galactagogue extract, measured 27 µm in diameter [46]. The findings demonstrate that the dimensions of CS-TPP microcapsules can fluctuate considerably, spanning from nanometers to micrometers, influenced by many parameters such as the concentrations of chitin, extract, and TPP. This study demonstrates that the particle size conforms to the specifications for microcapsules, which is significant as particle size directly influences other attributes, including release, stability, and biological activity. Meanwhile, the morphology of microcapsules should be crescent-shaped; however, not all of the microcapsules were spherical. This phenomenon arose from the physical and chemical qualities manifested during the microencapsulation process, resulting in differences in shape, surface, and size [37]. The spherical form arises from the surface tension that inherently develops during the creation of microcapsules [47]. The spherical form, permeable texture, and size discrepancies of the microcapsules stemmed from the interplay between the microencapsulation process parameters and the physical and chemical characteristics of the polymer (chitosan) and the cross-linking agent (TPP) [48]. This illustrates the significance of regulating process parameters to generate microcapsules with the requisite attributes for the intended use.

The success of encapsulation was subsequently evidenced by structural alterations observable using FTIR. **Figure 3** illustrates the variations in the spectra of the 3 samples: Chitosan and TPP as raw materials, and NLCE as the final product in this investigation. The chitosan spectrum exhibited peaks at 3,450 cm^{-1} (O-H stretching), 2,925 cm^{-1} (C-H stretching), 1,658 cm^{-1} (C=O stretching, amide I indicative of N-acetylglucosamine structure), 1,586 cm^{-1} (N-H bending vibrations representing N-acetylated residues), 1,417

cm^{-1} (N-H stretching, amide II associated with glucosamine functional groups), 1,390 cm^{-1} (N-H stretching, amide III), 1,143 cm^{-1} (C-O-C stretching), 1,036 cm^{-1} (C=O stretching), and 886 cm^{-1} (pyranose ring). The TPP spectrum exhibited 2 bands at 1,206 - 1,142 and 886 - 735 cm^{-1}, linked to the stretching vibrations of the P=O group in the phosphate ion; the band at around 552 cm^{-1} pertains to the distortion vibrations of P=O. In the NLCE, the amide I and II peaks were displaced to 1,627 and 1,542 cm^{-1}, respectively. Furthermore, the peak at 1,206 cm^{-1} (stretching vibrations of the P=O group) in the TPP spectrum changed to 1,315 cm^{-1} in the NLCE, signifying the cross-linkages between chitosan and TPP [23]. The NLCE exhibited bands at 1,095 cm^{-1}, corroborating the extract's existence in the NLCE. FTIR is crucial in confirming the creation of cross-links between polymers, hence demonstrating the successful synthesis of the NLCE. The absorption peaks of amides I and II in the NLCE, originally located at 1,658 and 1,417 cm^{-1} in chitosan, changed to 1,627 and 1,542 cm^{-1}, respectively. This signifies electrostatic interactions between the phosphate groups in TPP and the amine in chitosan [37].

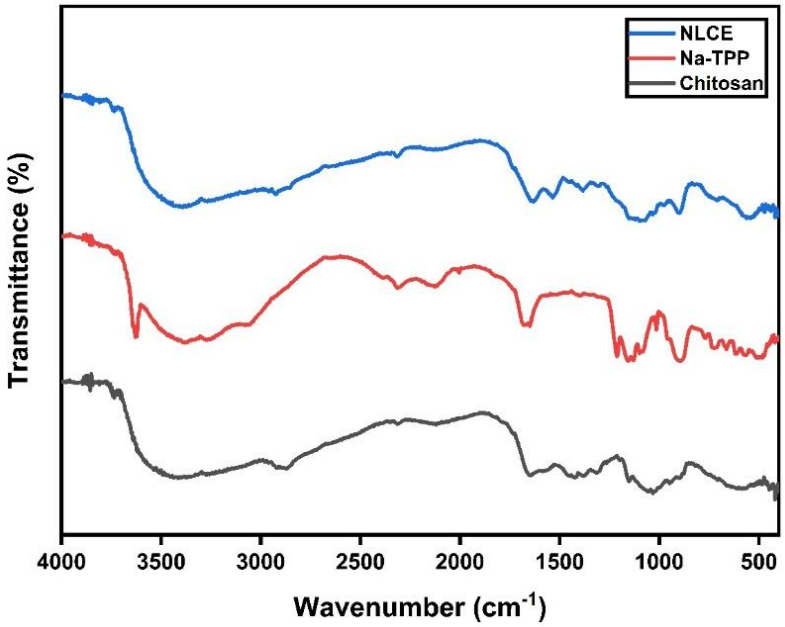

Figure 3 FTIR spectra of chitosan powder, Na-TPP, and NLCE.

Chemical compound analysis via LC-HRMS was conducted to verify the efficacy of encapsulation. The data presented in **Table 2** demonstrate that NLCE comprises many secondary metabolites originating from NL. Within the retention time interval of 5.2 - 5.8 min, a cluster of flavonoids exclusive to NL was identified, comprising hyperoside, miquelianin, and a quercetin derivative known as quercetin-xylosyl-glucoside. The existence of these peaks indicates that the primary phenolic constituents remain stable after encapsulation, potentially functioning as indicators for assessing the efficacy and release of active substances. The study identified the presence of erteberel at a retention time of 5.477 min, in the form of $[M + NH_4]^+$ ions, alongside flavonoids. The development of this ammonium adduct aligns with the utilization of a buffer containing ammonium salts in the mobile phase and suggests that neutral-basic substances can be detected more reliably using positive ionization mode. At RT 13.638 min, senkyunolide B was detected, signifying the presence of volatile-lactonic constituents from NL that were also encapsulated within the chitosan matrix. The LC-HRMS chemical profile indicates the efficacy of the encapsulating technology in preserving both polar and semipolar bioactive compounds. The data substantiate that the chitosan-TPP combination is an effective transporter for NL secondary metabolites.

Table 2 LC-HRMS data of compounds identified in NLCE.

RT (min)	Compound	Ion type	Formula	Molecular mass (Da)	m/z (observed)	Ionization mode
5.477	Erteberel	$[M + NH_4] + 1$	$C_{18}\ H_{18}\ O_3$	283.13	300.15	Positive
5.730	Hyperoside	$[M + H] + 1$	$C_{21}\ H_{20}\ O_{12}$	466.10	465.10	Positive
5.290	5,7-dihydroxy-2-(2,3,4-trihydroxyphenyl)-4H-chromen-4-one	$[M + H] + 1$	$C_{15}\ H_{10}\ O_7$	302.23	303.04	Positive
5.681	Miquelianin	$[M - H] - 1$	$C_{21}\ H_{18}\ O_{13}$	478.07	477.06	Negative
5.290	2-(3,4-Dihydroxyphenyl)-5,7-dihydroxy-4-oxo-4H-chromen-3-yl 6-O-β-D-xylopyranosyl-β-D-glucopyranoside	$[M + H] + 1$	$C_{26}\ H_{28}\ O_{16}$	596.05	597.14	Positive
13.638	Senkyunolide B	$[M + H] + 1$	$C_{12}\ H_{12}\ O_3$	206.08	205.08	Positive

RT (Retention time); m/z shows the mass-to-charge ratio of the detected ion.

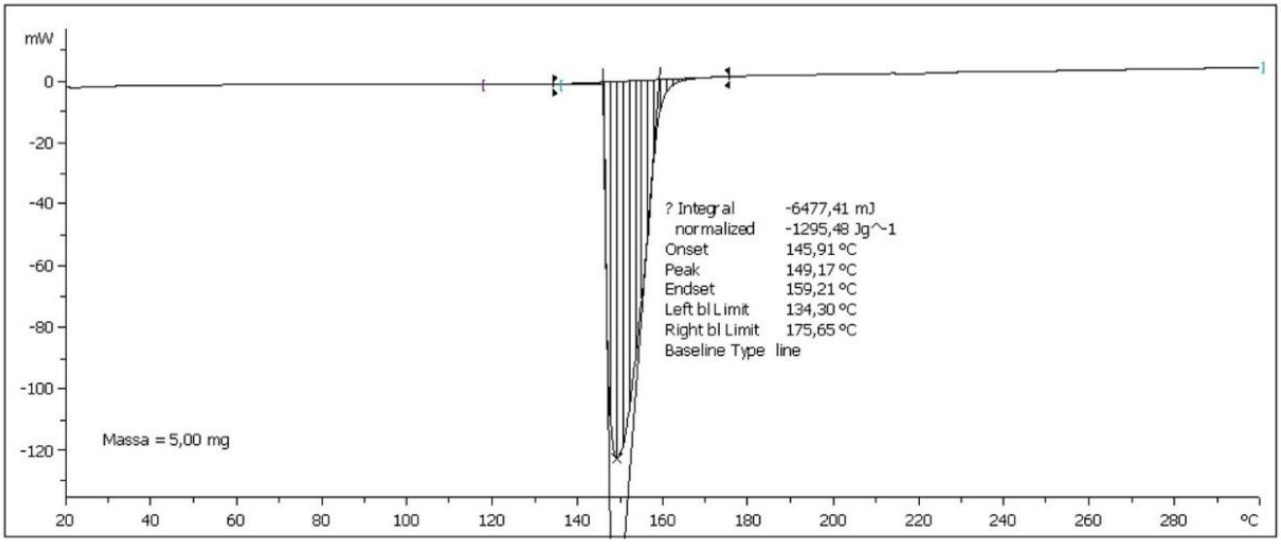

Figure 4 Differential scanning calorimetry (DSC) thermogram of NLCE showing a sharp endothermic peak at 149.17 °C, corresponding to the melting transition of encapsulated bioactive compounds. Data were obtained from 5.00 mg of the sample, indicating good thermal stability of the formulation.

The thermal properties of NLCE, as depicted in Figure 4 using DSC analysis, yield significant insights into the thermal features and interactions between bioactive chemicals and the polymer matrix. **Figure 4** presents a distinct endothermic peak, commencing at 145.91 °C, reaching a maximum at 149.17 °C, and concluding at 145.91 °C. The region beneath the curve, determined as the transition enthalpy (ΔH), is −1,295.48 J/g, signifying that the process is endothermic and entails a substantial energy change. This profile signifies a physical transition associated with the relaxation or melting of the semi-crystalline phase within the

composite system comprising chitosan, Na-TPP, and the bioactive component NL [49]. The lack of the distinct melting peak of flavonoids, typically observed between 140 - 160 °C, suggests that the bioactive molecules are likely not in a free crystalline state, but rather uniformly integrated within the chitosan matrix via hydrogen bonds and electrostatic interactions. This signifies the efficacy of the encapsulation procedure, as the active chemicals are both physically confined and linked to the polymer chains [50]. Moreover, the existence of a singular, comparatively large peak indicates the amorphous characteristics of the system, which is typically anticipated in nanoencapsulated formulations to enhance the solubility and bioavailability of the active constituents. The alteration in the transition temperature to approximately 149 °C, exceeding the melting point of various free phenolic constituents, indicates enhanced thermal stability resulting from the establishment of a crosslink network among the amino groups of chitosan, polyphosphate ions, and the hydroxyl/carboxyl groups of NL [29]. The DSC results affirm that NLCE possesses sufficient thermal stability and illustrate the efficacy of the encapsulation technique.

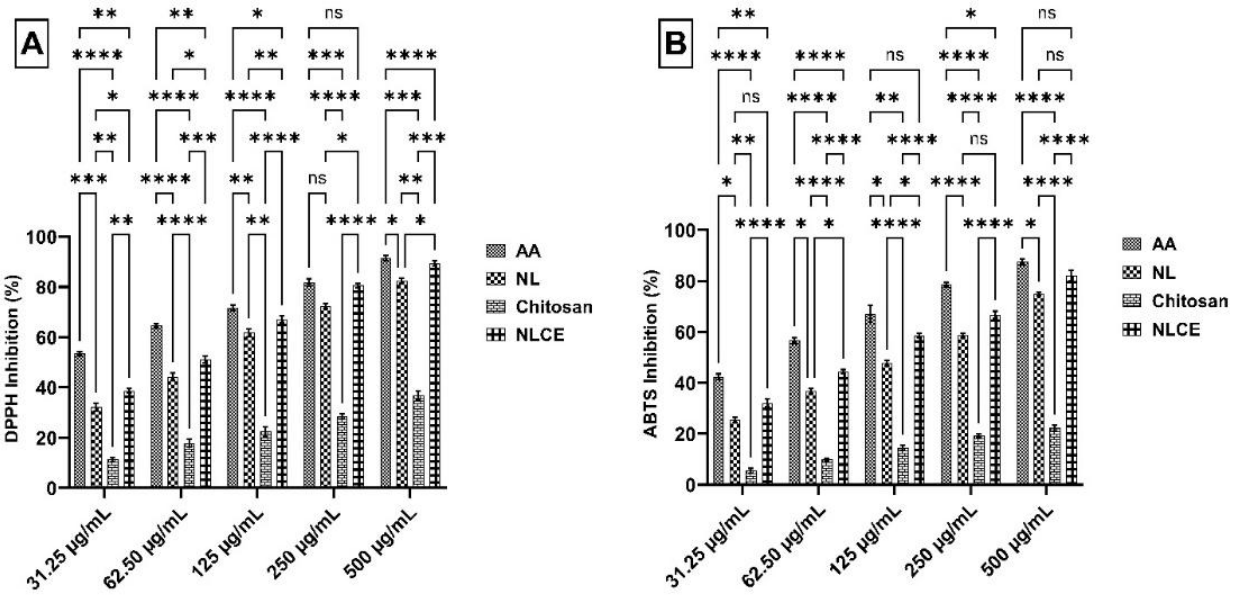

Figure 5 Radical scavenging effect of NLCE through (A) DPPH inhibition, (B) ABTS inhibition. Results are expressed as mean ± SD from triplicate experiments (n = 3). Statistical significance was determined using ANOVA followed by Tukey's post-hoc test. **** $p < 0.0001$, *** $p < 0.001$, ** $p < 0.01$, * $p < 0.05$, ^{ns} not significant.

Antioxidant activity of *N. nucifera* leaf extract-loaded chitosan encapsulates

Evaluation for antioxidant activity demonstrated that NLCE has significant radical scavenging capacity against DPPH and ABTS, as illustrated in **Figure 5**, in comparison to chitosan and NL. According to the DPPH inhibition data (**Figure 5(A)**) at concentrations ranging from 31.25 to 500 µg/mL, NLCE exhibited a progressive enhancement in inhibitory capacity correlating with concentration, yielding average values of 38.70 ± 0.94%, 51.11 ± 1.45%, 67.18 ± 1.40%, 80.48 ± 0.94%, and 89.45 ± 0.99%, respectively. This action surpassed that of NL at all dosages, but pure chitosan exhibited minimal inhibition (< 40% at 500 µg/mL). Ascorbic acid (AA), serving as a positive control, exhibited the highest activity (> 90% at 500 µg/mL). Two-way ANOVA revealed that both the treatment factor (AA, NL, chitosan, NLCE) and the concentration factor significantly influenced the inhibition % ($p < 0.0001$), with a notable interaction between the 2 ($p = 0.0022$). Tukey's post hoc test established that NLCE was substantially more effective than chitosan and NL across nearly all dosages, particularly within the 31.25 - 250 µg/mL range, with the disparity diminishing at the

highest dosage of 500 µg/mL. Concurrently, the outcomes of the ABTS radical assay exhibited a comparable pattern (**Figure 5(B)**). The NLCE inhibition percentage rose from 32.11 ± 1.52% at 31.25 µg/mL to 82.12 ± 2.19% at 500 µg/mL. This value surpasses that of NL (25.53 ± 1.06% to 74.90 ± 0.58%) and significantly exceeds that of chitosan (5.51 ± 0.88% to 22.19 ± 1.09%) at the identical concentration. AA had the greatest activity, ranging from 42.40 ± 1.10% to 87.44 ± 1.15%. Two-way ANOVA revealed a substantial impact of treatment and concentration ($p < 0.0001$), along with an interaction effect between the 2 ($p = 0.006$). Tukey's test indicated that NLCE exhibited significant differences from chitosan across all concentrations and generally outperformed NL, particularly at low to medium concentrations. The results validate that the encapsulation of *N. nucifera* leaf extract within a chitosan-TPP matrix can preserve and potentially augment antioxidant activity against DPPH and ABTS radicals. The enhanced activity mechanism is probably associated with the amorphous dispersion of phenolic chemicals within the matrix, as evidenced by DSC studies showing the absence of crystalline peaks in the extract [51]. This dispersion is believed to enhance the contact surface between bioactive chemicals and free radicals, therefore augmenting the accessibility of active sites for radical scavenging processes [52]. The comparatively minimal activity of chitosan indicates that the primary effect originates from the phytochemical constituents safeguarded within the encapsulating system, rather than from the polymer itself. Nonetheless, an alternative study indicates a synergistic interaction of the bioactive chemicals from NL and chitosan in radical inhibition. The addition of chitosan, which captures free radicals via interactions with its amine groups, enhances the radical suppression effect of the encapsulated extract [53].

Table 3 Inhibitory concentration 50 (IC_{50}) of several samples.

Sample	IC_{50} (µg/mL) ± SD				
	DPPH	**ABTS**	**Cytotoxic (24 h)**	**Cytotoxic (48 h)**	**Cytotoxic (72 h)**
NL	73.14 ± 4.09	118.24 ± 6.55	419.38 ± 12.58	282.68 ± 16.53	155.84 ± 6.67
Chitosan	> 500	> 500	> 500	> 500	> 500
NLCE	59.85 ± 1.90	74.96 ± 0.96	245.80 ± 12.57	155.23 ± 11.61	76.99 ± 3.55
AA	43.05 ± 0.85	53.70 ± 2.26	-	-	-
Dox	-	-	304.07 ± 36.98	126.36 ± 13.44	35.91 ± 4.30

NL (*N. nucifera* leaf extract), NLCE (*N. nucifera* leaf extract-loaded chitosan), AA (ascorbic acid), Dox (doxorubicin). A concentration test was conducted from 31.25 to 500 µg/mL.

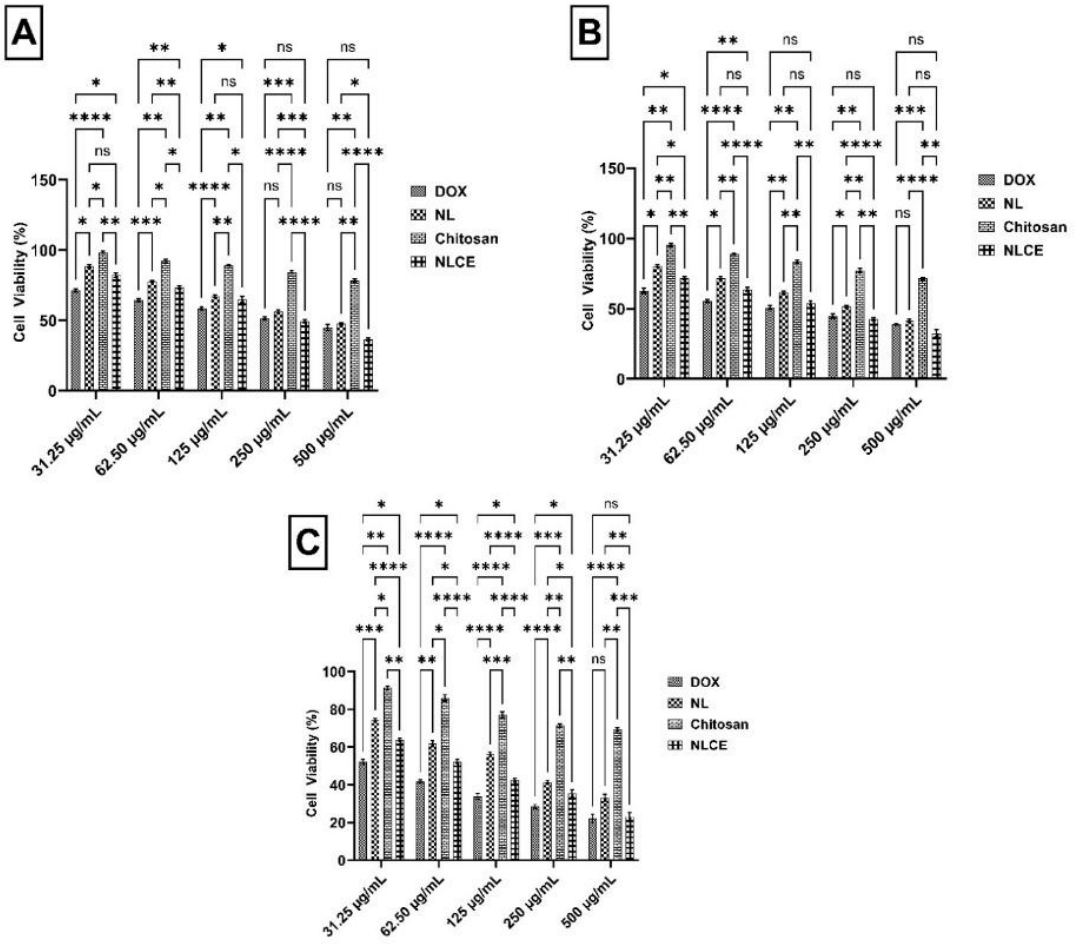

Figure 6 Cell viability (%) of MCF-7 cells after treatment with the sample test in various concentrations between 31.25 to 500 µg/mL. (A) 24 h incubation, (B) 48 h incubation, and (C) 72 h incubation. Results are expressed as mean ± SD from triplicate experiments (n = 3). Statistical significance was determined using ANOVA followed by Tukey's post-hoc test. **** $p < 0.0001$, *** $p < 0.001$, ** $p < 0.01$, * $p < 0.05$, ^{ns} not significant.

Subsequent study indicates that NLCE has significant radical scavenging ability against DPPH and ABTS, as seen by the Inhibitory Concentration $_{50}$ (IC_{50}) values presented in **Table 3**. In the DPPH assay, NLCE yielded an IC_{50} value of 59.85 ± 1.90 µg/mL, surpassing NL at 73.14 ± 4.09 µg/mL and chitosan at > 500 µg/mL. Concurrently, the AA standard exhibited the greatest activity, with an IC_{50} of 43.05 ± 0.85 µg/mL. A comparable trend was noted in the ABTS assay, wherein NLCE exhibited an IC50 of 74.96 ± 0.96 µg/mL, outperforming NL at 118.24 ± 6.55 µg/mL and chitosan at > 500 µg/mL. Nonetheless, the activity of NLCE remained inferior to that of AA, which measured 53.70 ± 2.26 µg/mL. The disparity in IC_{50} values between NLCE and NL signifies that the encapsulation inside the chitosan-TPP matrix not only safeguards the active compounds but also enhances the accessibility of hydroxyl groups from flavonoids and phenolic acids, which are integral to antioxidant action. Previous results, as noted by Fierri *et al.* [54], indicate that the antioxidant activity of encapsulated olive pomace extract in chitosan-TPP is enhanced in suppressing ABTS radicals compared to non-encapsulated forms. Fabrikov *et al.* [55] indicated that the antioxidant properties of tea polyphenols and epigallocatechin gallate in suppressing DPPH and ABTS radicals were enhanced following encapsulation with chitosan [55]. Lubis *et al.* [23] documented analogous results for the enhanced antioxidant activity of *Portulaca oleraceae* extract subsequent to encapsulation within a chitosan-TPP matrix [23]. These findings validate that NLCE exhibits superior antioxidant capacity compared to NL,

with efficacy nearing that of AA, especially in the DPPH assay. This advantage demonstrates that the chitosan-TPP-based nanoencapsulation system effectively preserves stability and enhances the efficacy of phenolic compounds, thereby presenting significant potential for use in the formulation of functional food products or natural pharmaceutical preparations.

Anti-breast cancer activity of *N. nucifera* leaf extract-loaded chitosan encapsulates

Cell viability assessment utilizing the MTT assay demonstrated that NLCE exhibited heightened cytotoxicity along with elevated concentration and prolonged incubation duration (Figure 6). After 24 h (**Figure 6(A)**), NLCE preserved a significant level of cell viability at low concentrations, exhibiting an average viability of 82.11 ± 1.45% at 31.25 µg/mL and 73.37 ± 1.01% at 62.5 µg/mL. Nonetheless, a substantial reduction occurred at > 125 µg/mL, with cell viability declining to 64.93 ± 2.24% at 125 µg/mL, 49.49 ± 1.10% at 250 µg/mL, and reaching a nadir of 36.21 ± 1.12% at 500 µg/mL. The reduction was significantly greater than that of chitosan, which preserved viability > 75% even at 500 µg/mL, and was more apparent than that of NL, which retained viability at 47.44 ± 0.89% at the highest concentration. Following a 48-hour incubation period (Figure 6B), the cytotoxic effect of NLCE became increasingly evident. Cell viability diminished to 71.56 ± 0.94% at 31.25 µg/mL and 63.70 ± 1.50% at 62.5 µg/mL. At a concentration of 125 µg/mL, viability was 54.10 ± 1.54%, thereafter declining to 42.39 ± 0.97% at 250 µg/mL and 32.44 ± 2.51% at 500 µg/mL. This trend indicates that prolonged contact enhances the infiltration and storage of bioactive chemicals within cells, leading to a more pronounced reduction in survival relative to NL and significantly more than chitosan. Thereafter, Dox as a positive control exhibited the highest activity, with a viability of merely 38.98 ± 0.58% at 500 µg/mL, underscoring the cell model's susceptibility to conventional chemotherapy. Subsequently, at 72 h (**Figure 6(C)**), the cytotoxic impact of NLCE attained its zenith. Cell viability was 63.84 ± 0.71% at 31.25 µg/mL, declining significantly to 52.34 ± 0.99% at 62.5 µg/mL and 42.48 ± 0.91% at 125 µg/mL. At elevated doses of 250 and 500 µg/mL, cell viability was recorded at 35.34 ± 2.00% and 23.11 ± 2.11%, respectively, signifying that about 3-quarters of the cell population lost their capacity for survival following prolonged exposure. Conversely, NL exhibited a comparable albeit diminished impact of 33.10 ± 1.95% at 500 µg/mL, whereas chitosan sustained over 69% efficacy even at the maximum dosage. Dox exhibited the most pronounced effect, demonstrating a viability of merely 22.14 ± 2.20% at 500 µg/mL, in alignment with its swift and direct cytotoxic action on cellular DNA. Furthermore, statistical analysis indicated that both the treatment component and the concentration factor significantly influenced cell viability at all time points ($p < 0.0001$). The Tukey test indicated that NLCE was consistently significantly distinct from chitosan across all dosages and showed more efficacy than NL, particularly at medium to high doses.

According to **Table 3**, the IC_{50} value of NLCE was measured at 245.80 ± 12.57 µg/mL at 24 h, declining to 155.23 ± 11.61 µg/mL at 48 h, and further diminishing to 76.99 ± 3.55 µg/mL at 72 h. This tendency signifies a notable temporal effect, wherein prolonged exposure facilitates the infiltration of bioactive components into cells, eliciting an enhanced cytotoxic response. In comparison to NL, which exhibited IC_{50} values of 419.38 ± 12.58; 282.68 ± 16.53; and 155.84 ± 6.67 µg/mL at 24, 48, and 72 h, respectively, NLCE had a consistently greater cytotoxic potential at all time intervals. This distinction verifies that the nanoencapsulation method not only safeguards the active substance but also enables regulated dispersion and release, hence augmenting its bioactivity against target cells. Conversely, pure chitosan demonstrated a considerably elevated IC_{50} (> 500 µg/mL) throughout all incubation durations, suggesting that the carrier polymer did not produce a notable hazardous effect at the evaluated concentrations. In contrast, as a positive control, Dox exhibited significantly higher efficacy with an IC_{50} of 304.07 ± 36.98 µg/mL at 24 h, diminishing to 126.36 ± 13.44 µg/mL at 48 h, and further to 35.91 ± 4.30 µg/mL at 72 h. Despite being more potent than NLCE, this notable disparity in activity is justifiable given that Dox is a synthetic chemotherapeutic agent with a targeted action against cancer cell DNA. These observations confirm that encapsulating NL in a chitosan-TPP matrix maintains bioactive components and increases antiproliferative activity against target cells in a time- and dose-dependent manner. This aligns

with a prior work by Sultana *et al.* [56], which showed that the efficacy of *Decalepis hamiltonii* extract against HeLa cells was enhanced following encapsulation with chitosan [56]. On the other hand, Devi *et al.* [57] indicated that rutin encapsulated with chitosan-TPP had considerably greater efficacy in suppressing PANC-1 cells compared to free rutin [57]. Thereafter, *Achillea goniocephala* extract loaded into chitosan increased the cytotoxic activity against HT-29 cancer cells to 80.40% compared to the extract without encapsulation of 43.59% [58]. Unfortunately, selectivity testing toward normal cells was not performed in this study. Nevertheless, it remains interesting to discuss how NLCE induces death in MCF-7 cells.

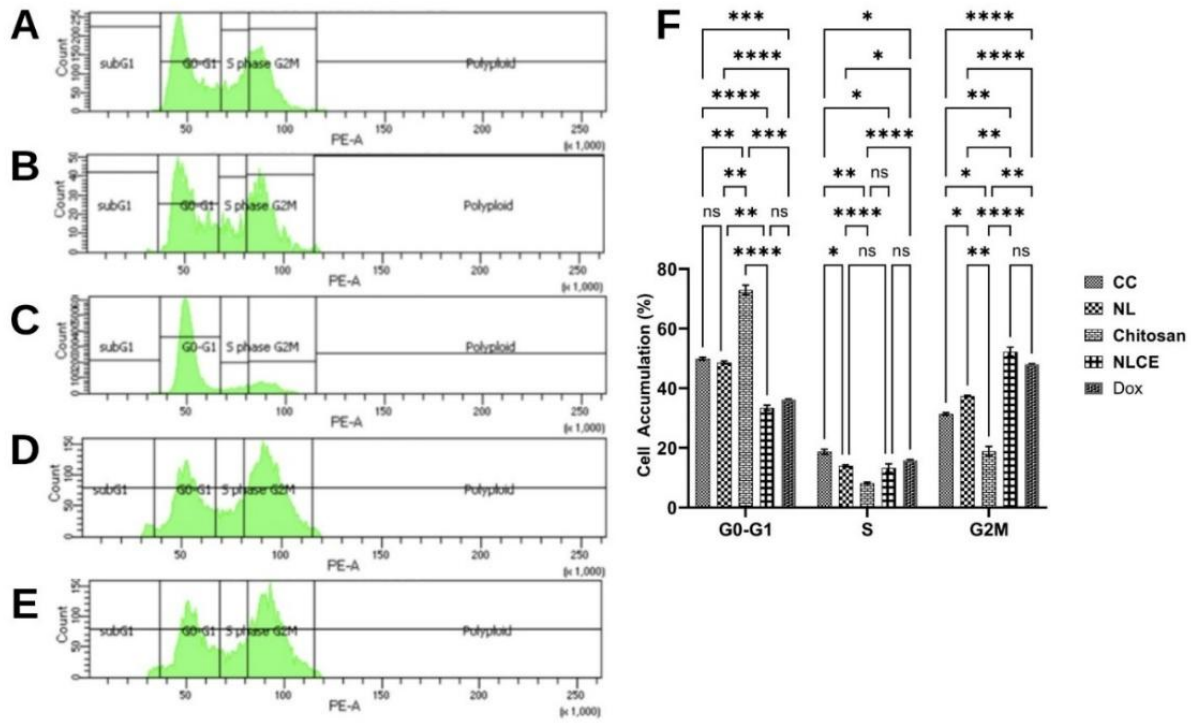

Figure 7 Cell cycle arrest induced effect after administration of the sample test at IC_{50}. (A) Control cell, (B) *N. nucifera* leaf extract, (C) Chitosan, (D) *N. nucifera* leaf extract-loaded chitosan encapsulates, (E) Doxorubicin, (F) cell accumulative (%). Results are expressed as mean ± SD from triplicate experiments (n = 3). Statistical significance was determined using ANOVA followed by Tukey's post-hoc test. **** $p < 0.0001$, *** $p < 0.001$, ** $p < 0.01$, * $p < 0.05$, ^{ns} not significant.

The flow cytometry test findings indicated that NLCE exposure resulted in significant alterations in cell cycle phase distribution relative to the control and other treatments (**Figure 7**). In control cells (**Figure 7(A)**), the predominant cell population was in the G_0/G_1 phase (49.90 ± 0.48%), succeeded by the G_2/M phase (31.38 ± 0.45%) and the S phase (18.71 ± 0.84%). NL exhibited a comparable trend (**Figure 7(B)**), with a minor reduction in the G_0/G_1 percentage (48.60 ± 0.50%) and an elevation in the G_2/M phase accumulation (37.40 ± 0.21%). Conversely, chitosan had a distinct effect (**Figure 7(C)**), the predominant fraction of cells resided in the G_0/G_1 phase (72.92 ± 1.60%), whereas the distributions in the S and G_2/M phases were merely 8.18 ± 0.32% and 18.86 ± 1.62%, respectively. The data indicate that chitosan does not significantly impede the late phase of the cell cycle. Exposure to NLCE resulted in a distinct distribution pattern (**Figure 7(D)**), characterized by a reduction in the proportion of cells in the G_0/G_1 phase to 33.44 ± 0.87% and a marginal decline in the S phase (13.26 ± 1.40%), however, the fraction in the G_2/M phase escalated significantly to 52.25 ± 1.49%. The predominant abundance of cells in the G_2/M phase signifies that NLCE can induce cell cycle arrest in this phase, hence inhibiting cells from progressing to mitosis. The results were nearly equivalent to the

positive control Dox (**Figure 7(E)**), which exhibited a distribution of 36.13 ± 0.23% in G_0/G_1, 15.81 ± 0.27% in the S phase, and 48.05 ± 0.15% in G_2/M. Statistical analysis with 2-way repeated measurements ANOVA demonstrated that the treatment factor significantly influenced cell accumulation in each phase ($p < 0.001$), although the column factor (cell cycle phase) exhibited no significant effect ($p > 0.05$). The interaction between the treatment factor and phase was significant ($p < 0.001$), demonstrating that each treatment influenced phase distribution differently. Tukey's post hoc test indicated that NLCE exhibited a significant difference from the control, chitosan, and NL in the G_2/M phase ($p < 0.01$), although it did not differ substantially from Dox, suggesting that the cell cycle suppression efficacy of NLCE was comparable to that of the positive control. The observations indicate that NLCE slows the cell cycle at the G_2/M phase, perhaps linked to the mechanisms of apoptosis induction or DNA damage that necessitate the G_2/M checkpoint for repair or cessation of cell growth. The results indicate that the chitosan-TPP encapsulation system preserves cytotoxic activity while simultaneously augmenting cell growth regulation mechanisms by inhibiting critical periods of the cell cycle.

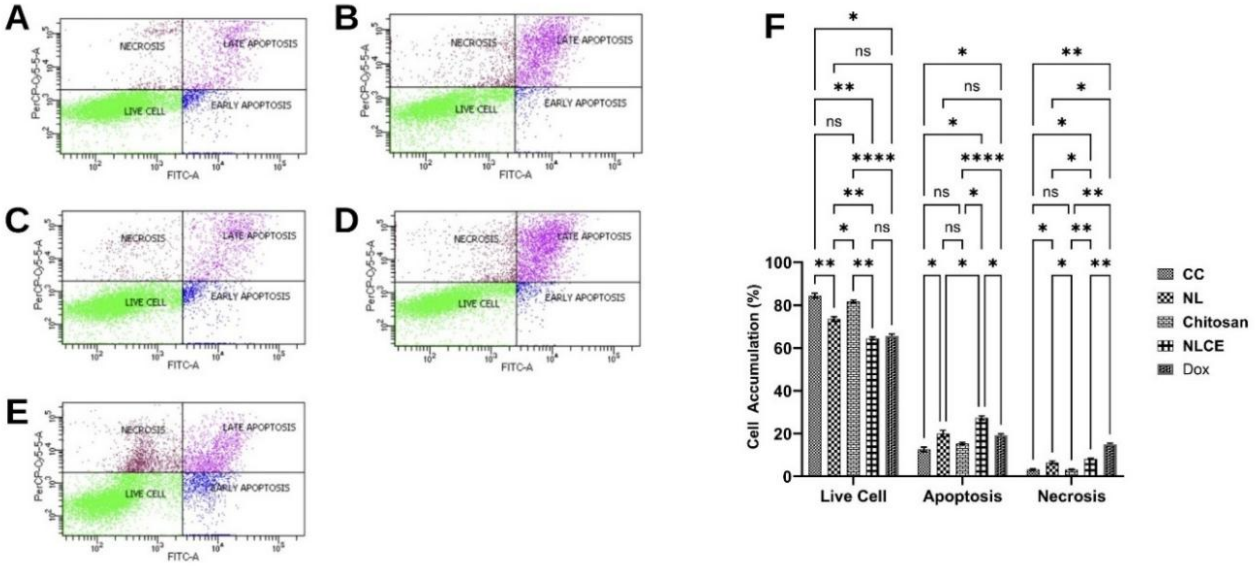

Figure 8 Apoptosis induced effect after administration of the sample test at IC_{50}. (A) Control cell, (B) *N. nucifera* leaf extract, (C) Chitosan, (D) *N. nucifera* leaf extract-loaded chitosan encapsulates, (E) Doxorubicin, (F) cell accumulative (%). Results are expressed as mean ± SD from triplicate experiments (n = 3). Statistical significance was determined using ANOVA followed by Tukey's post-hoc test. **** $p < 0.0001$, *** $p < 0.001$, ** $p < 0.01$, * $p < 0.05$, ^{ns} not significant.

Subsequently, flow cytometric analysis of apoptosis revealed that treatment with NLCE elevated the percentage of cells undergoing programmed cell death relative to the control and alternative treatments (**Figure 8**). In control cells (**Figure 8(A)**), the majority were viable (84.43 ± 1.08%), with only 12.60 ± 1.02% suffering apoptosis and 3.19 ± 0.44% undergoing necrosis. The administration of NL resulted in a marginal increase in apoptosis (±14%) (Figure 8B), although this difference was not statistically significant compared to the control. Chitosan exhibited a minimal apoptosis percentage (**Figure 8(C)**), consistent with the cytotoxicity test results, which indicated an IC_{50} value exceeding 500 µg/mL throughout all incubation durations. Conversely, NLCE diminished the proportion of viable cells to 69.62 ± 1.24% and markedly elevated the apoptosis rate to 25.31 ± 1.38%, although necrosis remained minimal at 5.07 ± 0.56% (**Figure 8(D)**). The results mirrored the pattern exhibited by Dox, which induced 27.15 ± 1.12% apoptosis (**Figure 8(E)**). The 2-way ANOVA statistical analysis demonstrated that the treatment factor exerted a highly significant influence

on the percentage of viable cells, apoptosis, and necrosis ($p < 0.001$). The Tukey test indicated that NLCE significantly differed from the control, chitosan, and NL in the apoptosis fraction ($p < 0.05$), but did not show a significant difference from Dox. The results align with the MTT cytotoxicity assay, indicating that NLCE exhibited an IC_{50} of 245.80 ± 12.57 µg/mL at 24 h, reducing to 155.23 ± 11.61 µg/mL at 48 h, and further to 76.99 ± 3.55 µg/mL at 72 h, significantly lower than the NL and chitosan. The observations corroborate that the enhancement of the cytotoxic effect of NLCE with time correlates with a heightened induction of apoptosis under prolonged exposure. Additionally, the results of cell cycle analysis corroborate this approach. NLCE induced a notable accumulation of cells in the G_2/M phase (52.25 ± 1.49%), accompanied by a reduction in the proportions of the G_0/G_1 and S phases. The arrest at the G_2/M checkpoint is a well-established mechanism that prevents cells from proceeding to mitosis, thereby providing an opportunity for DNA repair [59]. If the damage is irreparable, the cell will proceed to the apoptosis pathway [60]. The elevation of the G_2/M fraction, accompanied by a rise in apoptosis percentage in the NLCE treatment, suggests that the bioactive chemicals in NL within the chitosan-TPP matrix not only impede proliferation via cell cycle arrest but also induce programmed cell death. The amalgamation of viability data, cell cycle distribution, and apoptosis demonstrates that the antiproliferative mechanism of NLCE is contingent upon dosage and temporal factors. These findings underscore the promise of NLCE as a natural product with quantifiable anticancer efficacy and a defined mechanism. Consequently, assessments of PI3K and mTOR protein expression were conducted to clarify the mechanism by which NLCE functions as an anti-breast cancer agent.

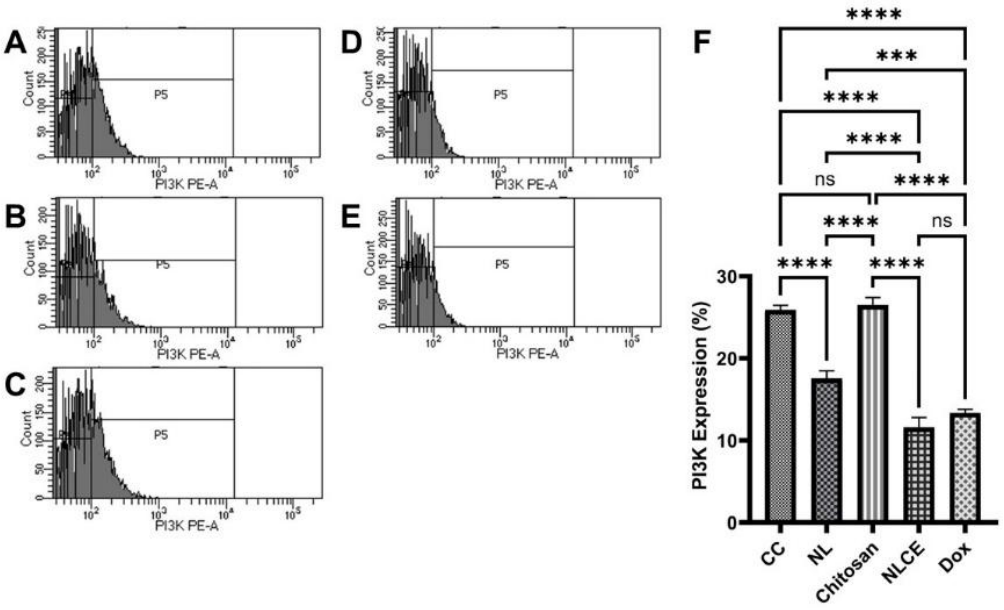

Figure 8 Flow cytometric analysis of PI3K protein expression following exposure to different treatments. (A) Control cell, (B) *N. nucifera* leaf extract, (C) Chitosan, (D) *N. nucifera* leaf extract-loaded chitosan encapsulates, (E) Doxorubicin, (F) PI3K expression (%). Results are expressed as mean ± SD from triplicate experiments (n = 3). Statistical significance was determined using ANOVA followed by Tukey's post-hoc test. **** $p < 0.0001$, *** $p < 0.001$, ^{ns} not significant.

The assessment of protein expression via flow cytometry revealed that treatment with NLCE resulted in a notable reduction in the expression of 2 key regulators of the proliferation pathway, specifically PI3K and mTOR, compared to the control and the majority of other treatments. In control cells, the mean expression of PI3K was 25.91 ± 0.54% (**Figure 8(A)**), whereas mTOR was 93.55 ± 1.03% (**Figure 9(A)**). The NL marginally decreased PI3K to 17.56 ± 0.90% (**Figure 8(B)**) and mTOR to 87.14 ± 0.30% (**Figure 9(B)**). Pure chitosan exhibited expression levels nearly equivalent to the control (PI3K 26.52 ± 0.88% (**Figure 8(C)**); mTOR 91.35 ± 0.98% (**Figure 9(C)**), suggesting that the polymer matrix had a negligible impact on this

pathway. Conversely, NLCE exhibited the most pronounced reduction in expression: PI3K decreased by 11.59 ± 1.20% (**Figure 8(D)**) and mTOR by 81.53 ± 0.99% (**Figure 9(D)**), nearing the levels observed with Dox therapy (PI3K 13.37 ± 0.42% (**Figure 8(E)**); mTOR 85.36 ± 0.60% (**Figure 9(E)**). The ANOVA analysis results indicated that the treatment exerted a highly significant impact on the expression of both proteins ($p < 0.0001$), while the Tukey test revealed that NLCE was considerably distinct from the control, chitosan, and NL in both parameters ($p < 0.001$). The disparity between NLCE and Dox was not significant for PI3K; however, for mTOR, the difference was minor yet statistically significant ($p = 0.0016$), suggesting that the effect of NLCE was substantially comparable to that of the positive control. Although flow cytometry analysis indicated a decreased fluorescence intensity of PI3K and mTOR, suggesting pathway inhibition, this interpretation should be considered preliminary. Further validation using molecular-level assays such as Western blot or RT-qPCR is necessary to confirm the precise regulatory effects of NLCE on the PI3K/mTOR signaling pathway.

Nonetheless, these findings align with the outcomes of the MTT cytotoxicity experiment, cell cycle analysis, and apoptosis evaluation. The reduction in PI3K/mTOR suggests that NLCE operates by modulating signaling pathways that govern cell proliferation, growth, and survival. Inhibition of the PI3K/mTOR pathway may result in a G_2/M phase arrest, as seen by the cell cycle distribution showing over 50% of cells in that phase. Upon failure of the G_2/M checkpoint to rectify the damage, cells are then driven towards the apoptotic pathway, which exhibited a considerable increase following NLCE treatment (25.31 ± 1.38%). This stratified process aligns with the reduction in cell viability and the gradual decline in IC_{50} over the incubation period. The studies demonstrate that NLCE reduces proliferation by driving cells into the G_2/M phase and alters the expression of critical proteins PI3K and mTOR to induce apoptosis and decrease cell survival. The suppression of the PI3K/mTOR pathway, induction of cell cycle arrest, and enhancement of apoptosis collectively elucidate the multi-target anticancer mechanism of NLCE, thereby reinforcing the potential use of this formulation as a natural product-based agent with defined and consistent biological efficacy.

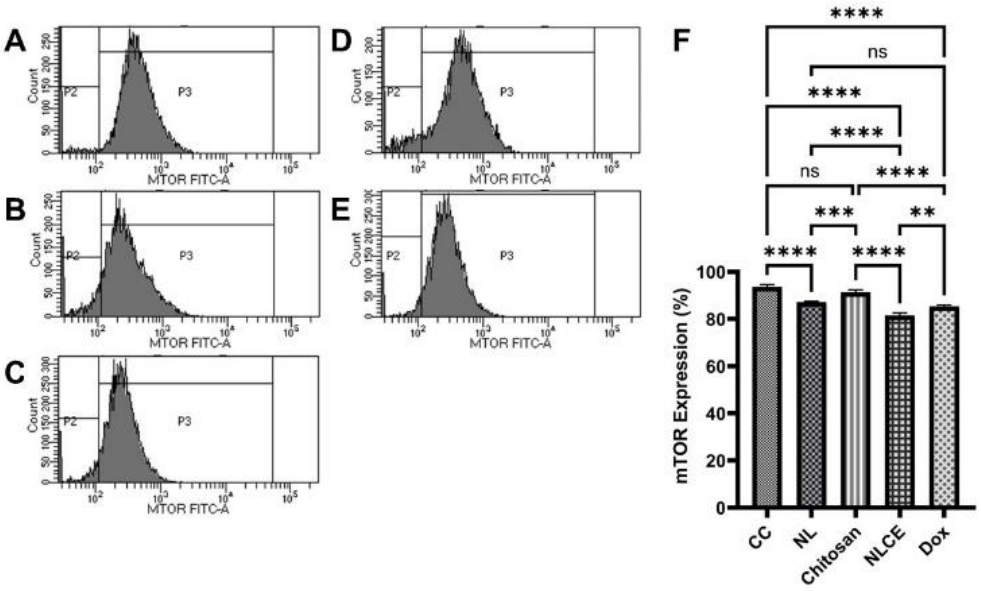

Figure 9 Flow cytometric analysis of mTOR protein expression following exposure to different treatments. (A) Control cell, (B) *N. nucifera* leaf extract, (C) Chitosan, (D) *N. nucifera* leaf extract-loaded chitosan encapsulates, (E) Doxorubicin, (F) PI3K expression (%). Results are expressed as mean ± SD from triplicate experiments (n = 3). Statistical significance was determined using ANOVA followed by Tukey's post-hoc test. **** $p < 0.0001$, *** $p < 0.001$, ** $p < 0.01$, ^{ns} not significant.

Numerous prior investigations have indicated that the anticancer properties of extracts encapsulated in a chitosan matrix are attributable to the secondary metabolites inside the extract and their synergistic interaction with the chitosan [61-63]. The encapsulation of active chemicals within the chitosan matrix enhances their stability and bioavailability, leading to more reliable anticancer efficacy. Chitosan possesses a positive charge at physiological pH, facilitating interactions with negatively charged cell surfaces and enhancing metabolite transport inside cells [64]. Moreover, hydrogen interactions established between chitosan and secondary metabolites impede the release of active chemicals and augment penetration across cell membranes [63]. Thus, anticancer efficacy may surpass that of freely supplied extracts. **Table 2** indicates that NLCE comprises various secondary metabolites known for their anticancer properties, including erteberel. Erteberel is an ERβ agonist, as reported by Belluti *et al.* [65], that has been evaluated in preclinical glioblastoma models, demonstrating chemotactic potential through processes involving IL-1β, which is beneficial for enhancing innate immunity against cancer [65]. Özistanbullu *et al.* [66] corroborate that the activation of ERβ by substances like erteberel will result in G2 arrest. Furthermore, Qiu *et al.* [67] found that hyperoside can trigger apoptosis in breast cancer via the ROS-mediated NF-κB signaling pathway. Liu *et al.* [68] support that hyperoside causes apoptosis and suppresses proliferation via the Caspase-3 and P53 signaling pathways in lung cancer. Miquelianin is a quercetin 3-O-glucuronide present in *N. nucifera*, and it does not negate the potential anti-breast cancer capabilities of quercetin [69]. According to Rivera *et al.* [70], quercetin induces cell cycle arrest by inhibiting mTOR. Jia *et al.* [71] demonstrated that quercetin impedes MCF-7 cell motility by obstructing glycolysis via the suppression of the Akt-mTOR pathway. Therefore, this study provides new insights into the nanoencapsulation of NL using the Chitosan-TPP ionic gelation system. While previous studies have mostly focused on encapsulation of other plant extracts, the present. work specifically utilized the NL, which is rich in flavonoids and polyphenols. Moreover, this is among the first reports demonstrating that such encapsulation enhances both antioxidant capacity and cytotoxic activity against MCF-7 cells through modulation of the PI3K/mTOR pathway. Thus, this study reveals the great potential of NLCE as an anti-breast cancer agent and its further development in biomedical applications.

Conclusions

In this study, the NL was successfully loaded into chitosan nanoparticles using an ionic gelation method and characterized by PSA, FTIR, SEM, LC-HRMS, and DSC. The particle size of NLCE was confirmed to the spherical in shape with a 350 nm particle size. In addition, the NLCE demonstrated stability at high temperatures and also contained several phytochemical compounds that have been shown to support the biological properties of NLCE. The biological properties of NLCE were strongly compared to NL and chitosan, including antioxidant activity via DPPH and ABTS radicals scavenging, cytotoxic and anti-proliferation test against MCF-7 cells, and thereafter, the mechanism of NLCE as an anti-breast cancer via cell cycle arrest and apoptosis induction via PI3K and mTOR protein inhibition. Nevertheless, this study has several limitations and warrants further investigation. Further work should focus on optimizing the encapsulation process to improve the physicochemical characteristics of NLCE and conducting *in vivo* studies to better illustrate its anti-breast cancer potential. Additionally, future studies should expand on the pharmacokinetic profile, toxicity assessment, and preclinical application of NLCE in cancer therapy.

Acknowledgements

This project has full support from Institut Kesehatan Helvetia, Indonesia and Universiti Sultan Zainal Abidin, Malaysia.

Declaration of Generative AI in Scientific Writing

During the preparation of this study, the authors used ChatGPT in order to verify the grammar and improve the readability. After using this tool/service, the authors reviewed and edited the content as needed and take full responsibility for the content of the article.

CRediT Author Statement

Khairani Fitri: Conceptualization, Methodology, Software, Investigation, Project administration, Writing

- original draft preparation; **Marwan Saad Azzubaidi:** Conceptualization, Supervision, Validation, Writing - Reviewing; **Nurulhuda Mat Hassan:** Supervision, Data curation, Formal analysis, Writing - Reviewing and Editing.

References

[1] X Zhao, R Zhao, X Yang, L Sun, Y Bao, YS Liu, A Blennow and X Liu. Recent advances on bioactive compounds, biosynthesis mechanism, and physiological functions of *Nelumbo nucifera*. *Food Chemistry* 2023; **412**, 135581.

[2] L Wang, Z Guan, S Li, X Dong, J Jiang, L Wang and S Xian. *Nelumbo nucifera* Gaertn. leaves: network pharmacology and molecular docking analysis of active ingredients and their mechanisms of action in treating atherosclerosis. *Biotechnology and Biotechnological Equipment* 2022; **36(1)**, 802-817.

[3] R Subashini and P Sumathi. Cardioprotective effect of *Nelumbo nucifera* on mitochondrial lipid peroxides, enzymes and electrolytes against isoproterenol induced cardiotoxicity in Wistar rats. *Asian Pacific Journal of Tropical Disease* 2012; **2**, S588-S591.

[4] H Du, JS You, X Zhao, JY Park, SH Kim and KJ Chang. Antiobesity and hypolipidemic effects of lotus leaf hot water extract with taurine supplementation in rats fed a high fat diet. *Journal of Biomedical Science* 2010; **17(S1)**, S42.

[5] X Ren, H Chen, H Wang, Y Wang, C Huang and H Pan. Advances in the pharmacological effects and mechanisms of Nelumbo nucifera gaertn. extract Nuciferine. *Journal of Ethnopharmacology* 2024; **331**, 118262.

[6] P Hu, X Ge, MT Gao, XZ Wang, YY Zhang, Y Li, J Xiao, YW Ni, QL Guo and Y Pan. Nelumbo nucifera Gaertn: An updated review of the antitumor activity and mechanisms of alkaloids. *Pharmacological Research - Modern Chinese Medicine* 2022; **2**, 100167.

[7] H Zhang, G Chen, Y Zhang, M Yang, J Chen and M Guo. Potential hypoglycemic, hypolipidemic, and anti-inflammatory bioactive components in Nelumbo nucifera leaves explored by bioaffinity ultrafiltration with multiple targets. *Food Chemistry* 2022; **375**, 131856.

[8] Z Wang, Y Cheng, M Zeng, Z Wang, F Qin, Y Wang, J Chen and Z He. Lotus (*Nelumbo nucifera* Gaertn.) leaf: A narrative review of its phytoconstituents, health benefits and food industry applications. *Trends in Food Science & Technology* 2021; **112**, 631-650.

[9] B Nutho and D Tungmunnithum. Exploring major flavonoid phytochemicals from *Nelumbo nucifera* Gaertn. as potential skin anti-aging agents: *In silico* and *in vitro* evaluations. *International Journal of Molecular Sciences* 2023; **24(23)**, 16571.

[10] MG Kamble, A Singh, SV Singh, MG Kamble, NA Sagar and N Rani. Nanotechnology for encapsulation of bioactive components: A review. *Discover Food* 2025; **5(1)**, 116.

[11] M Calderón-Oliver and E Ponce-Alquicira. The role of microencapsulation in food application. *Molecules* 2022; **27(5)**, 1499.

[12] ZA Raza, S Khalil, A Ayub and IM Banat. Recent developments in chitosan encapsulation of various active ingredients for multifunctional applications. *Carbohydrate Research* 2020; **492**, 108004.

[13] G Maleki, EJ Woltering and MR Mozafari. Applications of chitosan-based carrier as an encapsulating agent in food industry. *Trends in Food Science & Technology* 2022; **120**, 88-99.

[14] P Inthamat and U Siripatrawan. Influence of chitosan encapsulation on functionality and stability of astaxanthin nanoemulsion fabricated using high pressure homogenization. *International Journal of Biological Macromolecules* 2025; **303**, 140379.

[15] W Abd El-Fattah, A Guesmi, NB Hamadi, MR Abdulbaqi, A Shahat, RFM Elshaarawy and YA Hassan. Encapsulation of *Plicosepalus curviflorus*-derived polyphenols in chitosan-alginate microvehicles for potent anticancer uses: Optimization using response surface methodology. *International Journal of Biological Macromolecules* 2025; **320(2)**,145741.

[16] A Negi and KK Kesari. Chitosan Nanoparticle encapsulation of antibacterial essential oils. *Micromachines* 2022; **13(8)**, 1265.

[17] M Yousefi, E Khanniri, S Sohrabvandi, N Khorshidian and AM Mortazavian. Encapsulation of *Heracleum persicum* essential oil in chitosan

nanoparticles and its application in yogurt. *Frontiers in Nutrition* 2023; **10**, 1130425.

[18] MM Mondéjar-López, A Rubio-Moraga, AJ López-Jimenez, JCG Martínez, O Ahrazem, L Gómez-Gómez and E Niza. Chitosan nanoparticles loaded with garlic essential oil: A new alternative to tebuconazole as seed dressing agent. *Carbohydrate Polymers* 2022; **277**, 118815.

[19] Y Asres, A Hymete, H Admassu and A Ayalew. Characterization of microencapsulated *Thymus schimperi* essential oil prepared by spray and freeze-drying using gum arabic as carrier material. *Food Science & Nutrition* 2025; **13(7)**, e70604.

[20] G Morales-Olán, S Luna-Suárez, JDD Figueroa-Cárdenas, M Corea and M Rojas-López. Synthesis and characterization of chitosan particles loaded with antioxidants extracted from Chia (*Salvia hispanica* L.) seeds. *International Journal of Analytical Chemistry* 2021; **2021**, 5540543.

[21] CA Ukwubile, ND Menkiti and O Otalu. Chitosan nanoparticles encapsulating turmeric (*Curcuma longa*) extract for the management of Streptococcus agalactiae-associated breast cancer. *Asian Journal of Natural Product Biochemistry* 2025; **23(1)**, 19-26.

[22] K Fitri, MS Azzubaidi and NM Hassan. Optimization of polyphenol recovery and antioxidant activity from *Nelumbo nucifera* leaf using box-behnken design and LC-hrms profiling. *RASAYAN Journal of Chemistry* 2025; **18**, 1758-1772.

[23] LD Lubis, AT Prananda, NA Juwita, MA Nasution, RA Syahputra, S Sumaiyah, RR Lubis, MF Lubis, R Astyka and JF Atiqah. Unveiling antioxidant capacity of standardized chitosan-tripolyphosphate microcapsules containing polyphenol-rich extract of *Portulaca oleraceae*. *Heliyon* 2024; **10(8)**, e29541.

[24] S Sumaiyah, R Murwanti, DN Illian, MF Lubis and K Tampubolon. New insights of response surface methodology approach in optimizing total phenolic content of zanthoxylum acanthopodium DC. fruit extracted using microwave-assisted extraction and the impact to antioxidant activity. *Indonesian Journal of Chemistry* 2024; **24**, 1743-1759.

[25] G Diana, A Candiani, A Picco, A Milanesi, M Stampini, E Bari, ML Torre, L Segale and L Giovannelli. Chitosan for improved encapsulation of thyme aqueous extract in alginate-based microparticles. *International Journal of Biological Macromolecules* 2024; **270**, 132493.

[26] W Wang, J Jung and Y Zhao. Chitosan-cellulose nanocrystal microencapsulation to improve encapsulation efficiency and stability of entrapped fruit anthocyanins. *Carbohydrate Polymers* 2017; **157**, 1246-1253.

[27] MN Tabar, L Nateghi, MH Ravan and L Rashidi. Encapsulation of walnut husk and pomegranate peel extracts by alginate and chitosan-coated nanoemulsions. *International Journal of Biological Macromolecules* 2025; **301**, 140349.

[28] M Suryani, A Yulyana, S Sumaiyah, K Fitri, LD Lubis, W Daulay, C Surbakti, R Astyka and MF Lubis. Microwave-assisted extraction enhances the antioxidant and anti-diabetic activities of polyphenol-rich *Phyllanthus emblica* fruit extract. *Discover Food* 2025; **5**, 244.

[29] MF Lubis, R Murwanti, PAZ Hasibuan, S Sumaiyah, NA Juwita, A Yulyana, R Astyka, S Yuliasmi, LD Lubis, W Daula and K Fitri. The potential of natural deep eutectic solvent in polyphenol extraction of *Timonius flavescens* (Jacq) Baker as an anti-breast cancer agent and its toxicity evaluation. *Advances in Traditional Medicine* 2025; **5(1)**, 244.

[30] MF Lubis, H Syahputra, DN Illian and VE Kaban. Antioxidant activity and nephroprotective effect of *Lansium parasiticum* leaves in doxorubicin-induced rats. *Journal of Research in Pharmacy* 2022; **26**, 565-573.

[31] K Fitri, M Andry, TN Khairani, MA Nasution, AAC Bu'ulolo and MF Lubis. Antioxidant potential of ethanol extracts leaf and stem of *Nelumbo nucifera* Gaertn. with DPPH, ABTS, and frap methods. *Research Journal of Pharmacy and Technology* 2024; **17**, 6084-6090.

[32] MF Lubis, PAZ Hasibuan, VE Kaban and R Astyka. Phytochemicals analysis and cytotoxic activity of *Lansium domesticum* Corr extract-cisplatin combination against PANC-1 cell line. *Rasayan Journal of Chemistry* 2023; **16(1)**, 32-37.

[33] MF Lubis, PAZ Hasibuan, H Syahputra, JM Keliat, VE Kaban and R Astyka. Duku (*Lansium domesticum*) leaves extract induces cell cycle arrest and apoptosis of HepG2 cells via PI3K/Akt pathways. *Trends in Sciences* 2023; **20(2)**, 6437-6437.

[34] PPAZ Hasibuan, JM Keliat and MF Lubis. Combination of cisplatin and ethyl acetate extract of Vernonia amygdalina Delile induces cell cycle arrest and apoptosis on PANC-1 cells via PI3K/mTOR. *Journal of Pharmacy & Pharmacognosy Research* 2024; **12**, 870-880.

[35] PAZ Hasibuan, JM Keliat, MF Lubis and A Nasution. The ethyl acetate extract of Vernonia amygdalina leaf ameliorates gemcitabine effect against migration and invasion of PANC-1 cells via down-regulation the VEGF, COX2, and RAS/MEK pathways. *Saudi Pharmaceutical Journal* 2024; **32(1)**, 101872.

[36] K Essifi, M Lakrat, D Berraaouan, ML Fauconnier, AE Bachiri and A Tahani. Optimization of gallic acid encapsulation in calcium alginate microbeads using box-behnken experimental design. *Polymer Bulletin* 2021; **78(10)**, 5789-5814.

[37] M Yousefi, N Khorshidian, AM Mortazavian and K Khosravi-Darani. Preparation optimization and characterization of chitosan-tripolyphosphate microcapsules for the encapsulation of herbal galactagogue extract. *International Journal of Biological Macromolecules* 2019; **140**, 920-928.

[38] JO Akolade, HOB Oloyede, MO Salawu, AO Amuzat, AI Ganiyu and PC Onyenekwe. Influence of formulation parameters on encapsulation and release characteristics of curcumin loaded in chitosan-based drug delivery carriers. *Journal of Drug Delivery Science and Technology* 2018; **45**, 11-19.

[39] B Zhao, Z Yang, Z Li and B Niu. Encapsulation of curcumin in chitosan-phytic acid (CS-PA) capsule: Bioavailability, simulated gastrointestinal digestion, and colonic fermentation *in vitro*. *Food Bioscience* 2025; **68**, 106612.

[40] A Vaseghi, RA Parchin, KR Chamanie, M Herb, H Maleki and M Sadeghizadeh. Encapsulation of propolis extracted with methylal in the chitosan nanoparticles and its antibacterial and cell cytotoxicity studies. *BMC Complementary Medicine and Therapies* 2014; **24(1)**, 165.

[41] ES Kim, Y Baek, HJ Yoo, JS Lee and HG Lee. Chitosan-tripolyphosphate nanoparticles prepared by ionic gelation improve the antioxidant activities of astaxanthin in the *in vitro* and *in vivo* model. *Antioxidants* 2022; **11(3)**, 479.

[42] T Jiang, Y Wang, Z Yu and L Du. Synthesis, characterization of chitosan/tripolyphosphate nanoparticles loaded with 4-chloro-2-methylphenoxyacetate sodium salt and its herbicidal activity against *Bidens pilosa* L. *Scientific Reports* 2024; **14(1)**, 18754.

[43] NC da Silva, OBG Assis, AG de Oliveira Sartori, SM de Alencar and M Martelli-Tosi. Chitosan suspension as extractor and encapsulating agent of phenolics from acerola by-product. *Food Research International* 2022; **161**, 111855.

[44] E Sánchez-Hernández, A Santiago-Aliste, A Correa-Guimarães, J Martín-Gil, RJ Gavara-Clemente and P Martín-Ramos. Carvacrol encapsulation in chitosan–carboxymethylcellulose-alginate nanocarriers for postharvest tomato protection. *International Journal of Molecular Sciences* 2024; **25**, 1104.

[45] SM Hosseini, H Hosseini, MA Mohammadifar, AM Mortazavian, A Mohammadi, K Khosravi-Darani, S Shojaee-Aliabadi, S Dehghan and R Khaksar. Incorporation of essential oil in alginate microparticles by multiple emulsion/ionic gelation process. *International Journal of Biological Macromolecules* 2013; **62**, 582-588.

[46] N Khorshidian, A Mahboubi, N Kalantari, H Hosseini, M Yousefi, M Arab, AG da Cruz, AM Mortazavian and FS Mahdavi. Chitosan-coated alginate microcapsules loaded with herbal galactagogue extract: Formulation optimization and characterization. *Iranian Journal of Pharmaceutical Research* 2019; **18**, 1180-1195.

[47] X Teng, M Zhang, AS Mujumdar and H Wang. Garlic essential oil microcapsules prepared using gallic acid grafted chitosan: Effect on nitrite control of prepared vegetable dishes during storage. *Food Chemistry* 2022; **388**, 132945.

[48] A Kumar, A Singh and J Sheikh. Boric acid crosslinked chitosan microcapsules loaded with

frankincense oil for the development of mosquito-repellent, antibacterial, antioxidant, and flame-retardant cotton. *International Journal of Biological Macromolecules* 2023; **248**, 125874.

[49] N Khorshidian, A Mahboubi, N Kalantari, H Hosseini, M Yousefi, M Arab, AG da Cruz, AM Mortazavian and FS Mahdavi. Hollow microcapsule with pH-sensitive chitosan/polymer shell for *in vitro* delivery of curcumin and gemcitabine. *European Polymer Journal* 2022; **162**, 110887.

[50] MH Sultan, SS Moni, OA Madkhali, MA Bakkari, S Alshahrani, SS Alqahtani, NA Alhakamy, S Mohan, M Ghazwani, HA Bukhary, Y Almoshari, A Salawi and M Alshamrani. Characterization of cisplatin-loaded chitosan nanoparticles and rituximab-linked surfaces as target-specific injectable nano-formulations for combating cancer. *Scientific Reports* 2022; **12(1)**, 468.

[51] O Chongsrimsirisakhol and T Pirak. Polyphenol release and antioxidant activity of the encapsulated antioxidant crude extract from cold brew spent coffee grounds under simulated food processes and an *in vitro* static gastrointestinal model. *Foods* 2023; **12(5)**, 1000.

[52] M Peanparkdee, C Borompichaichartkul and S Iwamoto. Bioaccessibility and antioxidant activity of phenolic acids, flavonoids, and anthocyanins of encapsulated Thai rice bran extracts during *in vitro* gastrointestinal digestion. *Food Chemistry* 2021; **361**, 130161.

[53] F Canbolat, N Demir, OT Yayıntas, M Pehlivan, A Eldem, TK Ayna and M Senel. Chitosan nanoparticles loaded with quercetin and valproic acid: A novel approach for enhancing antioxidant activity against oxidative stress in the SH-SY5Y human neuroblastoma cell line. *Biomedicines* 2024; **12(2)**, 287.

[54] I Fierri, R Chignola, C Stranieri, EG Di Leo, M Bellumori, S Roncoletta, A Romeo, F Benetti, AMF Pasini and G Zoccatelli. Formulation, characterization, and antioxidant properties of chitosan nanoparticles containing phenolic compounds from olive pomace. *Antioxidants* 2024; **13(12)**, 1522.

[55] D Fabrikov, ÁT Varga, MCV García, P Bélteky, G Kozma, Z Kónya, JL López Martínez, F Barroso and MJ Sánchez-Muros. Antimicrobial and antioxidant activity of encapsulated tea polyphenols in chitosan/alginate-coated zein nanoparticles: A possible supplement against fish pathogens in aquaculture. *Environmental Science and Pollution Research* 2024; **31**, 13673-13687.

[56] S Sultana, HJ Shwetha, MN Jayakumar, TR Lakshmeesha, AM Raichur and T Ravikiran. Chitosan-assisted delivery of *Decalepis hamiltonii* extract for improved anticancer efficacy in HeLa cell lines. *International Journal of Biological Macromolecules* 2025; **319**, 145359.

[57] KKTR Devi, SJ Paulraj, Y Shah, SR Kumar and P Kejamurthy. Chitosan-tripolyphosphate nanoparticles encapsulated rutin targeting bacterial growth inhibition and its cytotoxicity on PANC-1 pancreatic adenocarcinoma cell. *Journal of Applied Pharmaceutical Science* 2023; **13**, 141-148.

[58] D Taşkın, M Doğan, M Ermanoğlu and T Arabaci. *Achillea goniocephala* extract loaded into nanochitosan: *In vitro* cytotoxic and antioxidant activity. *Clinical and Experimental Health Sciences* 2021; **11**, 659-666.

[59] SM Abdelnasser and N Abu-Shahba. *Bacillus sonorinses* derived exopolysaccharide enhances cell cycle arrest, apoptosis, necrosis, autophagy and COX-2 down regulation in liver cancer cells. *Biotechnology Reports* 2024; **43**, e00848.

[60] L Xiong, N Deng, B Zheng, T Li and RH Liu. Goji berry (Lycium spp.) extracts exhibit antiproliferative activity via modulating cell cycle arrest, cell apoptosis, and the p53 signaling pathway. *Food & Function* 2021; **12**, 6513-6525.

[61] FM Almutairi, AA Abd-Rabou and MS Mohamed. Raloxifene-encapsulated hyaluronic acid-decorated chitosan nanoparticles selectively induce apoptosis in lung cancer cells. *Bioorganic & Medicinal Chemistry* 2019; **27(8)**, 1629-1638.

[62] X Xu, Q Li, W Dong, G Zhao, Y Lu, X Huang and X Liang. Cinnamon cassia oil chitosan nanoparticles: Physicochemical properties and anti-breast cancer activity. *International Journal of Biological Macromolecules* 2023; **224**, 1065-1078.

[63] G Rajivgandhi, S Kadaikunnan, G Ramachandran, G Chackaravarthi, CK Chelliah, M

Maruthupandy, M Natesan, F Quero and WJ Li. Anti-cancer ability of chitosan nanoparticles loaded plant essential oil evaluated against A549 human lung cancer cells through invitro approaches. *Journal of King Saud University-Science* 2023; **35**, 102598.

[64] CA Ukwubile, TS.Malgwi and CE Odu. Targeted delivery of *Zingiber officinale* Roscoe extract-loaded chitosan nanoparticles for inhibition of multidrug-resistant Escherichia coli-induced HCT-116 colon cancer. *Clinical Phytoscience* 2025; **11(1)**, 6.

[65] S Belluti, C Imbriano and L Casarini. Nuclear estrogen receptors in prostate cancer: From genes to function. *Cancers* 2023; **15(18)**, 4653.

[66] D Özistanbullu, R Wilhelm, G Reichenbach, M Doll, K Bahrami, N Zöller, F Schnütgen, A König, T Scheller, L Winkler, P Spahn, M Jäger, JP Nicolay, J Pfeilschifter, B Schilling, R Kaufmann, A Koch, S Kippenberger, J Kleemann and M Meissner. Estrogen receptor β stimulation as a possible novel therapeutic target for cutaneous T-cell lymphoma. *Blood Advances* 2025; **9**, 2651-2662.

[67] J Qiu, T Zhang, X Zhu, C Yang, Y Wang, N Zhou, B Ju, T Zhou, G Deng and C Qiu. Hyperoside induces breast cancer cells apoptosis via ROS-mediated NF-κB signaling pathway. *International Journal of Molecular Sciences* 2020; **21(1)**, 131.

[68] Y Liu, G Liu, J Mei and J Wang. The preventive effects of hyperoside on lung cancer *in vitro* by inducing apoptosis and inhibiting proliferation through Caspase-3 and P53 signaling pathway. *Biomedicine & Pharmacotherapy* 2016; **83**, 381-391.

[69] A Bishayee, PA Patel, P Sharma, S Thoutireddy and N Das. Lotus (*Nelumbo nucifera* Gaertn.) and its bioactive phytocompounds: A tribute to cancer prevention and intervention. 2022; **14(3)**, 529.

[70] A Rivera Rivera, L Castillo-Pichardo, Y Gerena and S Dharmawardhane. Anti-breast cancer potential of quercetin via the AkT/AMPK/mammalian target of rapamycin (mTOR) signaling cascade. *PLoS One* 2016; **11(6)**, e0157251.

[71] L Jia, S Huang, X Yin, Y Zan, Y Guo and L Han. Quercetin suppresses the mobility of breast cancer by suppressing glycolysis through Akt-mTOR pathway mediated autophagy induction. *Life Sciences* 2018; **208**, 123-130